Meso-β-scale Characteristics of an Episode of Meso-α-scale Convective Complexes

RAY L. MCANELLY AND WILLIAM R. COTTON

Colorado State University, Department of Atmospheric Science, Fort Collins, CO 80523

(Manuscript received 30 November 1984, in final form 28 March 1986)

ABSTRACT

A variety of meso-β-scale (20–200 km, <6 h) temporal and spatial characteristics associated with the life-cycle of the meso-α-scale (200–2000 km, >6 h) convective complex (MCC) are described. The analysis is based on a typical episode of MCCs in the central United States. Thunderstorms in the MCC are generally well-organized into meso-β-scale convective features. The larger MCCs are typically preceded by several of these meso-β convective clusters or bands, which tend to be aligned along linear meso-α-scale features such as the eastern slope of the Rockies or thermodynamic discontinuities evident in hourly surface or satellite data. The intense development of these larger systems involves the growth, merger and interaction of those meso-β convective features located nearest the intersection of the meso-α axes along which they are aligned. Throughout the mature phase of the MCC, multiple meso-β convective components may persist within the more uniform meso-α cloud shield as expanding regions of stratiform anvil precipitation develop. The decay of the system is marked by the weakening and difluent propagation of its meso-β convective components. Hourly precipitation data reveal a characteristic precipitation life-cycle in relation to the MCC's satellite appearance. These typical meso-β-scale characteristics offer potential tools for the short-range forecasting of MCCs and their hydrological consequences.

1. Introduction

The midlatitude *m*esoscale *c*onvective *c*omplex (MCC) has been identified and described by Maddox (1980) as a unique class of convection, organized on the meso-α scale (200–2000 km, >6 h),[1] which accounts for much of the nocturnal precipitation and severe weather over a large portion of the central United States during the convective season. The predominantly nocturnal occurrence of thunderstorms in this area has been long established (Kincer, 1916; Wallace, 1975), and previous attempts to characterize their mesoscale organization (Porter et al., 1955; Miller, 1972) have generally invoked the more widely recognized quasi-two-dimensional squall line conceptual model (Palmen and Newton, 1969; Lilly, 1979). However, guided by the view offered by geostationary satellite (upon which the MCC's definition is based), Maddox (1983) and Fritsch and Maddox (1981) demonstrated with composited synoptic rawinsonde data that the "average" MCC has distinctly different structural and dynamical characteristics from the severe, prefrontal squall line. Climatologically, this distinction relates to severe squall lines being a predominantly springtime, baroclinic phenomenon (e.g., Bluestein and Jain, 1985), while MCCs occur from spring on throughout the summer, often in a more barotropic environment (Maddox, 1983).

The composite studies of Maddox (1983) and Fritsch and Maddox (1981), as well as several individual case studies of MCCs or closely related events (Bosart and Sanders, 1981; Maddox and Doswell, 1982; Wetzel et al., 1983), suggest that the MCC is in many larger-scale respects more akin to the oceanic tropical cloud cluster (Gray and Jacobsen, 1977; McBride, 1981; McBride and Zehr, 1981) than to the meso-α-scale squall line. The emerging view of the cloud cluster (e.g., Houze and Betts, 1981) emphasizes the existence of a deep mesoscale "anvil" cloud, which produces about 40% of the cluster's total rainfall. A mesoscale circulation involving midlevel inflow, descent beneath the anvil, and ascent within the anvil has been convincingly demonstrated to be as integral to the system as the embedded convective-scale circulations and precipitation, which are generally concentrated on the leading edge of the system. Fritsch and Maddox (1981) used numerical model support to infer that a similar, convectively forced mesoscale region of mean ascent in the mid-to-upper troposphere is a fundamental aspect of the MCC. This meso-α ascent explains many of the MCC's features, including the extensive cloud shield and large area of light, stratiform precipitation.

Because MCCs have only recently been recognized, there has not yet emerged a generalized view of their internal structure and evolution. Despite their generalized, large-scale distinction from the midlatitude squall line, several studies indicate that there is much overlap in their substructure and dynamics. For instance, meso-β-scale (20–200 km, <6 h) circulations

[1] See Orlanski (1975) for a detailed discussion of scale terminology.

© 1986 American Meteorological Society

similar to those described above have been diagnosed in the vertical plane across midlatitude squall lines (Newton, 1966; Sanders and Emanuel, 1977; Ogura and Chen, 1977; Ogura and Liou, 1980). Smull and Houze (1985) showed that Ogura and Liou's (1980) Oklahoma squall line was also an MCC. That case and a western Texas MCC studied by Leary and Rappaport (1983) both had a leading convective region and trailing stratiform region that resembled the structure of tropical cloud clusters (Zipser, 1977; Leary and Houze, 1979). In contrast, a dual MCC event investigated by Rockwood et al. (1984) exhibited a more complex substructural evolution in which the precipitation patterns differed from that of cloud clusters.

More generalized studies by Clark et al. (1980) and Merritt and Fritsch (1984) also indicate that MCCs are a broad class of systems with much variability in their internal structure and evolution, related in part to characteristic synoptic settings. A composite study by Kane et al. (1985) shows how the "average" MCC's precipitation, when averaged over such variability, is spatially and temporally distributed.

Cotton et al. (1983) and Wetzel et al. (1983) investigated a complex MCC as it evolved up-scale from its initial convective roots over the central Colorado Rockies to its early weakening stages in northeastern Kansas. That case occurred within an 8-day episode during which one or more MCCs occurred each evening over the central United States. This paper is an expanded study of that MCC episode, concentrating on various phenomenological meso-β-scale aspects of MCC evolution. The episode is briefly discussed in Section 2. The data and analysis techniques are described in section 3. In section 4, we describe qualitatively the meso-β-scale substructure and evolution of the larger MCCs, emphasizing a degree of similarity that expands previous conceptual models of the MCC life cycle. Quantitative hourly precipitation characteristics of the episode's MCCs are then described in section 5, revealing a characteristic precipitation signature in relation to their satellite appearance.

2. Cases studied

As evidenced by the accumulating climatological data based on MCCs (e.g., Rodgers et al., 1985), successive MCCs (and less organized mesoscale convective systems) often develop daily over a several-day period when a slowly evolving large-scale circulation pattern becomes favorable for their formation. The MCCs studied here occurred within such an 8-day episode, 3–10 August 1977, in which afternoon and evening convection developed up-scale each day into one or more MCCs that persisted well into or through the night. The tracks of the mesoscale convective systems which attained MCC dimensions are shown in Fig. 1, where the darkened tracks indicate periods when the cloud shields met Maddox's (1980) areal and thermal criteria for a mature MCC.

The quasi-stationary large-scale pattern which set up this episode is discussed in Cotton et al. (1983) and Wetzel et al. (1983). It basically featured a zonal polar jet along the United States/Canadian border, a quasi-stationary surface front from Colorado to the Great Lakes and New England (Fig. 1), maritime tropical southerly flow to the south of the front, and an apparent extension of a monsoonal circulation over the southwestern United States, which brought a southwesterly influx of Pacific moisture over the central Rockies to the High Plains.

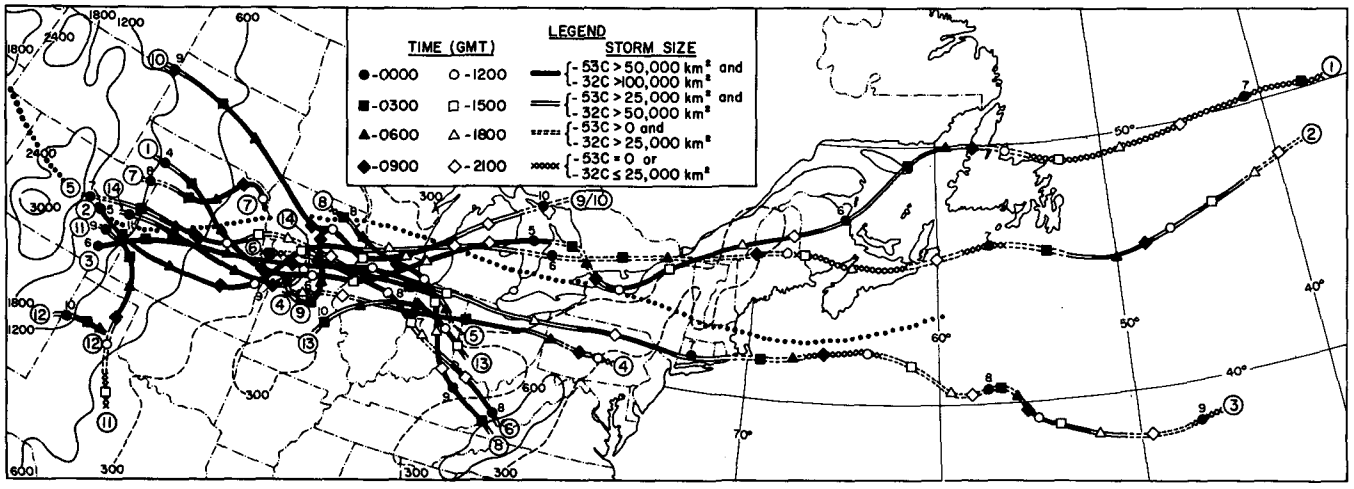

FIG. 1. Tracks of the centroids of the 14 mesoscale convective systems which attained MCC dimensions (darkened track) during the episode of 3–10 August 1977, based on 3-h interval analysis of geosynchronous, infrared satellite data. Circled system numbers at the beginning and end of the tracks indicate the chronological order of their initial appearances. The date is given near each 0000 GMT symbol. The mean 8-day position of the quasi-stationary surface front (derived from 00, 06, 12 and 18 GMT NWS surface maps) is indicated by the dotted curve. Smoothed terrain heights are indicated by solid contours at 600-m intervals and the dashed 300-m contour. (Adapted from Wetzel et al., 1983).

Several general aspects of the MCC episode can be inferred from Fig. 1. Two distinct MCC genesis regions are evident, one along the eastern slopes of the Rockies and High Plains ("western" systems), and the other further east over the more level and lower terrain of Missouri and Iowa ("eastern" systems). The MCCs tended to occur in the vicinity of, and track along, the quasi-stationary front. The remnants of decayed complexes persisted for long periods (up to 3 days) as identifiable regions of loosely organized convection and anvil cloud, which occasionally reintensified into mature complexes. The 8-day rainfall over the eastern two-thirds of the United States was strongly dominated by these systems (see Fig. 2 of Wetzel et al., 1983).

3. Data and analysis methodology

a. Satellite data and analysis

The life-cycles of the 12 best-organized MCCs from the episode were quantified using "MB-enhanced" infrared (IR) GOES satellite imagery (Clark, 1983). Figure 2 illustrates the evolution of the first MCC of the episode as seen in GOES-East imagery. Enhanced fea-

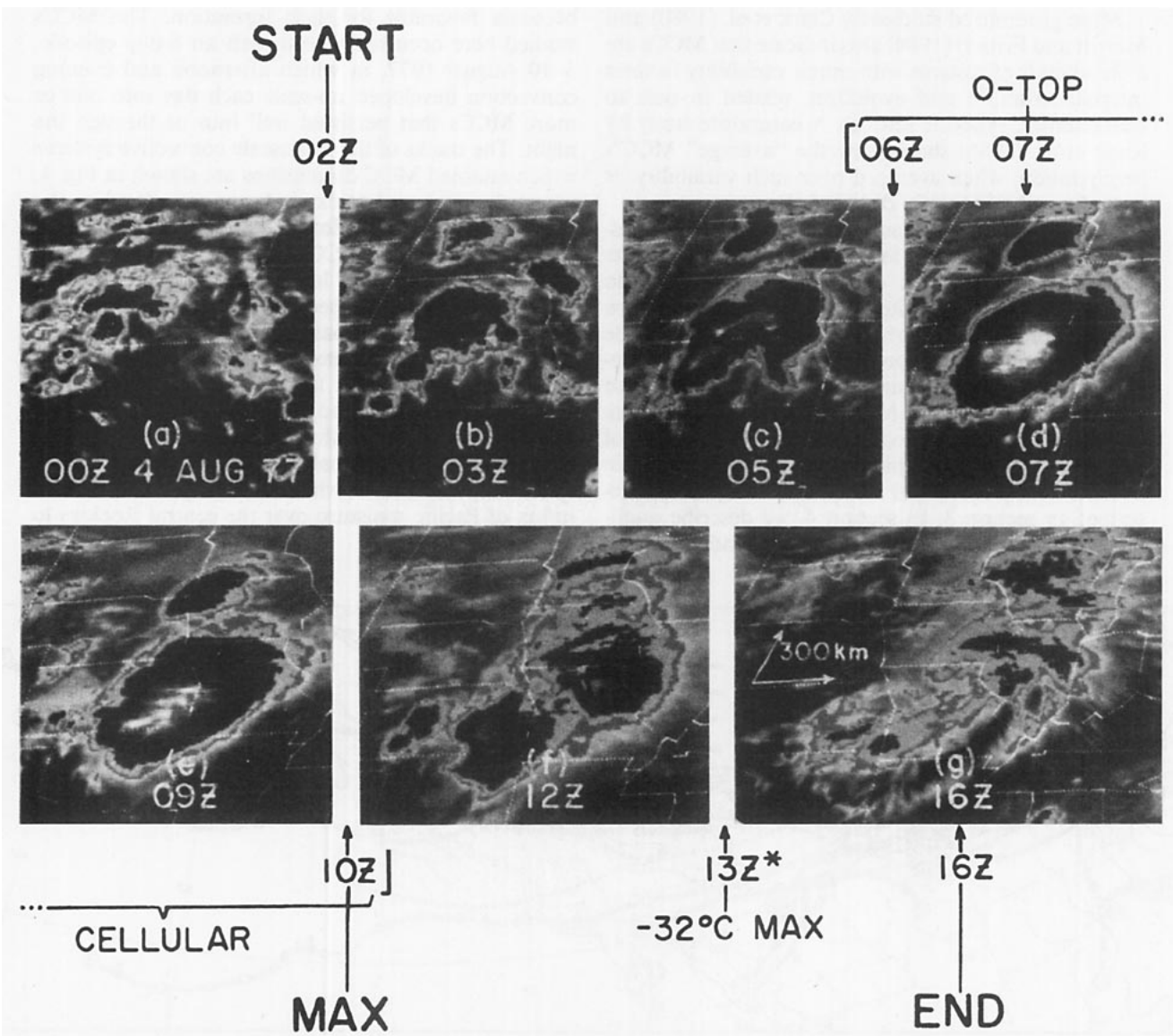

FIG. 2. Enhanced IR GOES-East satellite images spanning the life cycle of the western MCC number 1 through the night of 3–4 Aug 1977. Central standard time is 6 h earlier than the indicated GMT time. The stepped shapes of medium gray, light gray, dark grey and black are thresholds for areas with IR temperatures colder than −32°, −42°, −53° and −59°C, respectively. Temperatures progressively colder than −63°C appear as a gradual black-to-white shade. The grid in the 09 GMT image is positioned about 150 km too far northward. A distance scale is indicated over Nebraska in (g). The life-cycle terminology is described in the text.

tures utilized in this study are the IR isotherms of −32° and −53°C (following Maddox, 1980) and the light-shaded interior anvil regions that are indicative of overshooting thunderstorm activity (Clark, 1983).

In order to relate the satellite-viewed storm systems to other meteorological fields, we first manually remapped these features from approximately hourly-interval images onto standard meteorological working maps. On-the-hour GOES-East imagery provided the best vantage and most complete dataset, and was thus used when available; otherwise, images at 30 min (GOES-East) or 15 min (GOES-West) off the hour were remapped. In the analysis of the MCCs' substructures (Section 4), these IR maps were used for the display and interpretation of the associated radar fields. In the more quantitative precipitation analysis (section 5), we used the working maps to derive an hourly record of IR areas colder than −32° and −53°C for each MCC. These planimetric measurements yielded on-the-hour areas either directly, or by interpolation from off-the-hour IR maps. Considering the errors due to navigation, remapping and planimetry, the accuracy of the IR areas is sufficient for their limited quantitative applications.

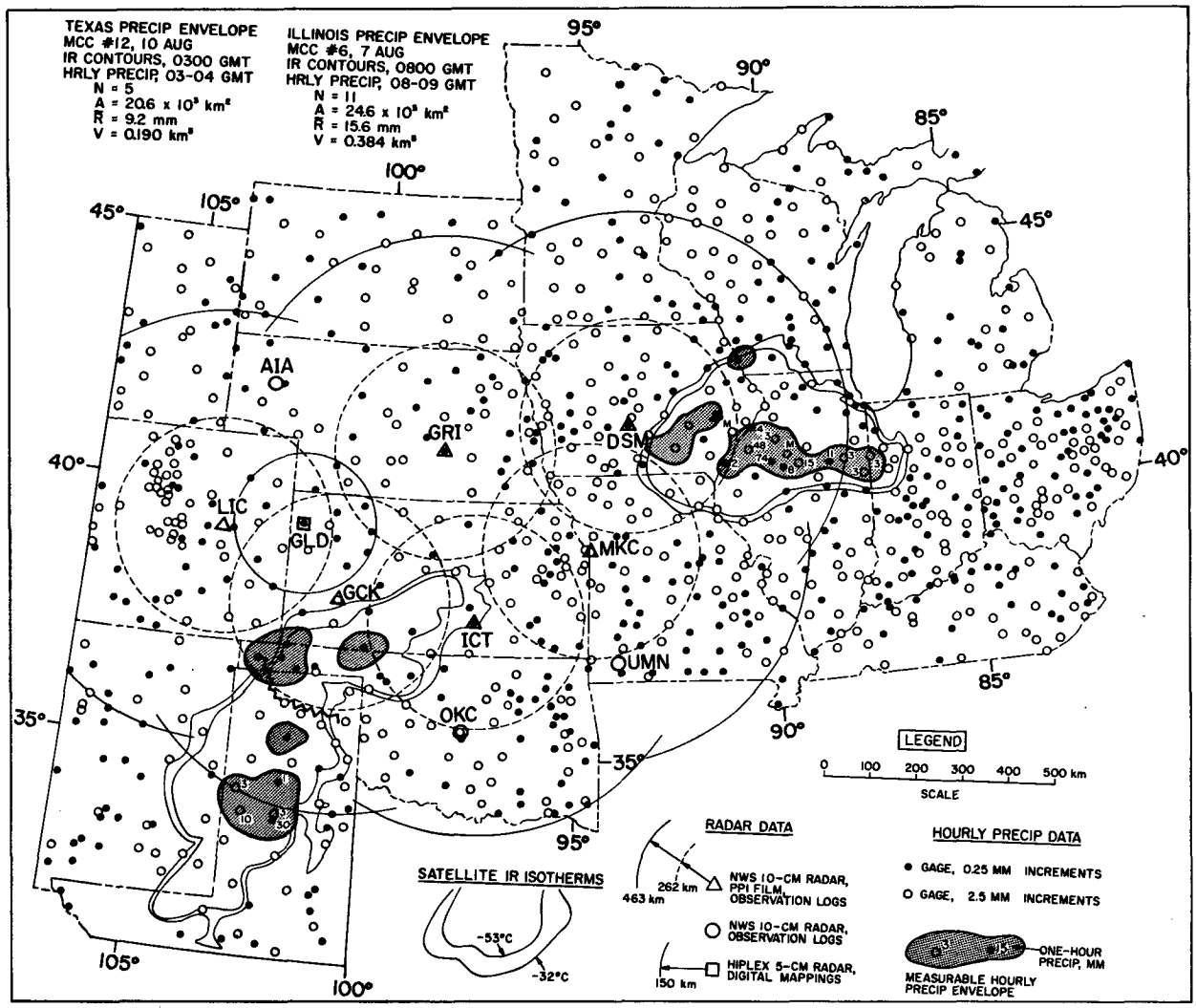

FIG. 3. Radar and hourly precipitation networks over the MCC study area (refer to legend in figure for plotting conventions). PPI film was acquired from the six National Weather Service WSR-57 (10-cm) radars at Limon, CO (LIC), Grand Island, NE (GRI), Des Moines, IA (DSM), Garden City (GCK), and Wichita (ICT), KS, and Kansas City, MO (MKC). Their maximum ranges and higher-resolved coverages are indicated. Radars at GCK and MKC had VIP display capability. Radar observation logs were obtained from these six sites and the NWS radar sites at Alliance, NE (AIA), Oklahoma City, OK (OKC), and Monett, MO (UMN). Also used were 5-cm radar data from the HIPLEX site at Goodland, KS (GLD). Operable sites of two types of recording raingages are indicated. Examples are shown of hourly rainfall envelopes associated with the eastern MCC number 6 and the western MCC number 12, whose remapped IR cloud shields are indicated. For each MCC, an example of calculating an hourly envelope's area (A), average rainfall ($\bar{R}$) and volume (V) from its number (N) of measurable reports is given.

TABLE 1. Meso-α-scale statistics of the 12 MCCs studied quantitatively, stratified by genesis region and by maximum anvil size into four composite categories.

	Large MCCs					Small MCCs			
	Maximum IR area (10^3 km^2)					Maximum IR area (10^3 km^2)			
Number	−53°C	−32°C	Mature duration (h)	Total rainfall volume (10^{-3} km^3)	Number	−53°C	−32°C	Mature duration (h)	Total rainfall volume (10^{-3} km^3)
				Western MCCs					
1	340	611	14	4867	5a	101	218	9	109
2	252	383	16	6075	11	86	155	7	289
3	238	386	13	6049	12	138	208	8	855
Western large average	277	460	14.3	5664	Western small average	108	194	8.0	418
				Eastern MCCs					
6	239	354	10	3540	4	108	167	7	2516
8	307	562	13	8213	5b	89	132	6	323
9/10	307	522	9	6964	9	139	227	9	1221
Eastern large average	284	479	10.7	6239	Eastern small average	112	175	7.3	1353

Of greater impact than those errors was the subjective determination of what constituted an MCC's anvil in the first place. Usually, it was unambiguously defined by an isolated, contiguous IR cloud shield, as typified in Fig. 3 by the remapped MCC over eastern Iowa and northern Illinois. Occasionally, however, we grouped multiple IR areas where anvil merging or splitting occurred, as with the two large −53°C areas in Fig. 2f. Other times, it seemed most reasonable to subjectively define an MCC boundary along a relative warm axis between a cloud shield that clearly underwent a quasi-circular "MCC-like" life-cycle, and a contiguous, "non-MCC" IR appendage which never became an organized part of the system. The most extreme case of such a situation is illustrated in Fig. 3, where the MCC over the Texas panhandle was deemed to be distinct from the attached cloud shield on its northeast flank. While such problems might raise questions concerning the "purity" of our cases, we believe our MCC case selection and definition are totally in accord with the rationale behind the stringent, arbitrary criteria adopted by Maddox (1980).

Based on the hourly IR measurements, we define the mature MCC to "start" when the contiguous area within the −53°C IR isotherm first exceeds 50 000 km^2, to reach its "maximum" when this area attains its largest size, and to "end" when this area first becomes less than 50 000 km^2 (at 0200, 1000 and 1600 GMT,[2] respectively, for MCC number 1 in Fig. 2). The mature duration is defined as the time elapsed from "start" to "end". Although Maddox (1980) used both −32 and −53°C IR areas as criteria for these MCC benchmarks, our analysis of hourly precipitation data shows that most of the rainfall occurs within the colder area, whereas the −32°C area is largely nonprecipitating anvil. Therefore, we have based these definitions solely on the −53°C area.

In addition to these areally-defined points in the life cycle, a meso-α "cellular" stage is defined more subjectively as the period after the system has apparently unified into a single meso-α "cell" and during which the −53°C IR contour is relatively smooth and circular.[3] In Fig. 2, for instance, contrast the unified, meso-α "cellular" appearance at 0700 and 0900 GMT with the more jagged −53°C appendages before, and the more ragged −53°C edges afterward. Within the "cellular" stage, the time of maximum "overshooting-top" activity is defined subjectively as when the light-shaded anvil interior reaches its largest and coldest extent (0700 GMT in Fig. 2). These points in the life cycle were determined to the nearest hour.

Life cycles were determined in this manner for the 12 MCCs listed in Table 1. Note from Fig. 1 that system number 5 had two mature periods, first as a western MCC (number 5a), and again as an eastern MCC when it reintensified in eastern Iowa (number 5b). Similarly, system number 9/10, depicted in Fig. 1 as a merging track in Iowa, developed between and adjoined the pre-

[2] Central standard time is 6 h earlier than the universal time convention used throughout this paper.

[3] Such a meso-α "cell", or circulation, should not be confused with convective-scale cells. Maddox (1980) describes this meso-α, unicellular satellite appearance as indicative of "a focused, central region of meso-α-scale upward motion in the middle and upper portions of the troposphere."

existing western MCC number 10 and eastern MCC number 9.

b. Radar data and analysis

In Section 4, the radar echo structures of the large MCCs listed in Table 1 are described, based on data from the radar network depicted in Fig. 3. The data base consisted of plan-position indicator (PPI) film and observation logs from the National Weather Service (NWS) WSR-57 (10-cm) radars; NWS operational hourly radar depiction maps and Manually Digitized Radar maps (Moore et al., 1974); and 5-min digitized mappings of composite PPIs and echo-top PPIs (Schroeder and Klazura, 1978), processed from 5-cm radar volume scans collected at Goodland, Kansas, under the Bureau of Reclamation's High Plains Experiment (HIPLEX).

In terms of quantitative analysis applications, these data were very limited for many reasons. Chief among these were the antiquated status of the NWS radar network; the marginal photographic quality of the NWS PPIs; the great preponderance of the PPIs being low-elevation scans; and differences in sensitivity (especially in detecting smaller precipitation particles), attenuation effects, and PPI data content between the NWS and HIPLEX radars. Because of these limitations, our radar analysis is qualitative: we emphasize only the meso-β-scale organization of convection within MCCs and persistent, widespread areas of stratiform precipitation, as inferred from low-level echo structure.

Our analysis procedure consisted of producing hourly working maps of areally composited radar data at about 25 min after the hour, which was near the time that NWS hourly radar observations were made. At the expense of nonconcurrence between the IR and radar maps, this time was chosen in order to take full advantage of the observation logs. Features manually mapped onto the working charts included the outlines of all echoes, and axes and cores of stronger convective echoes, from the NWS and HIPLEX PPIs; higher-intensity reflectivity contours that were available from the HIPLEX PPIs, from the two NWS radars having Video Integrator Processor (VIP) intensity displays, and from occasional PPIs with reduced receiver gain; and the information on the radar logs (intensities and heights of cells, cell and area movements, etc.). The frequency of frames on the PPI film (about one every 5 min) provided excellent temporal resolution between the hourly composite maps.

In producing and analyzing the hourly radar maps, a wide variety of convective-scale structure, organization and propagation modes was evident. These ranged from unorganized multicell systems to well-defined meso-β squall lines, and approached isolated supercells.[4] Regardless of its convective-scale structure (and often the poor data quality precluded such detail), the strong convection was predominantly organized into meso-β-scale clusters or bands that persisted for well over an hour. Such meso-β convective features are thus the basic unit of the MCC's substructure that we describe in relation to the evolving IR cloud shield. Each schematic meso-β convective feature depicted in the analyses of section 4 may represent almost total echo coverage, or alternatively, simply a cluster or line of discrete echoes that displays a pronounced temporal continuity. Some areas of weak echo and isolated or short-lived echoes have been omitted from the schematic structures if they had little apparent effect on the MCC's cloud shield.

Also included in the schematic radar analyses in section 4 are widespread, persistent areas of stratiform echo that produced measurable hourly precipitation. It should be emphasized that very weak echo and elevated layers of anvil precipitation, which might not reach low-level scanning angles, are not included in the analyses.

c. Hourly precipitation data and composite analysis methodology

The description of the temporal evolution of the MCC's precipitation characteristics (section 5) is based on an analysis of hourly precipitation data,[5] recorded by the hydrological network depicted in Fig. 3. Considering the long duration of an MCC relative to the hourly sampling period, and the large area affected by its rainfall, this network provides much detail on the MCC's meso-β-scale rainfall characteristics. However, there are problems inherent in its sampling of MCC rainfall: its inability to representatively sample convective-scale rainfall; its nonuniform station spacing, which is particularly sparse on the western plains; and its use of both weighing gages (from which hourly accumulations are rounded to the nearest 0.25 mm) and coarser-resolution tipping-bucket gages (which count the number of accumulations reaching 2.5 mm each hour). These problems have prompted us to adopt a composite analysis approach, in which the precipitation data for the 12 individual MCCs in Table 1 are condensed into four composite categories of three similar systems each: western large (W-L), western small (W-S), eastern large (E-L) and eastern small (E-S) MCCs. The W-L and E-L MCCs had maximum anvil areas about 2.5 times larger, and durations longer, than their smaller counterparts (Table 1).

The procedure for quantifying the rainfall data for the individual MCCs consisted first of plotting reports for each hour onto the corresponding map of $-32°$ and $-53°$C IR isotherms. Contiguous areas of rainfall, which generally corresponded closely to the meso-β convective features, were then enclosed into precipi-

[4] Such convective-scale detail is beyond the scope of this paper. See Kessler (1982) for a review of the structure, organization and dynamics of thunderstorms.

[5] "Hourly Precipitation Data" is published monthly by the National Climatic Data Center, NOAA/NESDIS, Asheville, NC 28801.

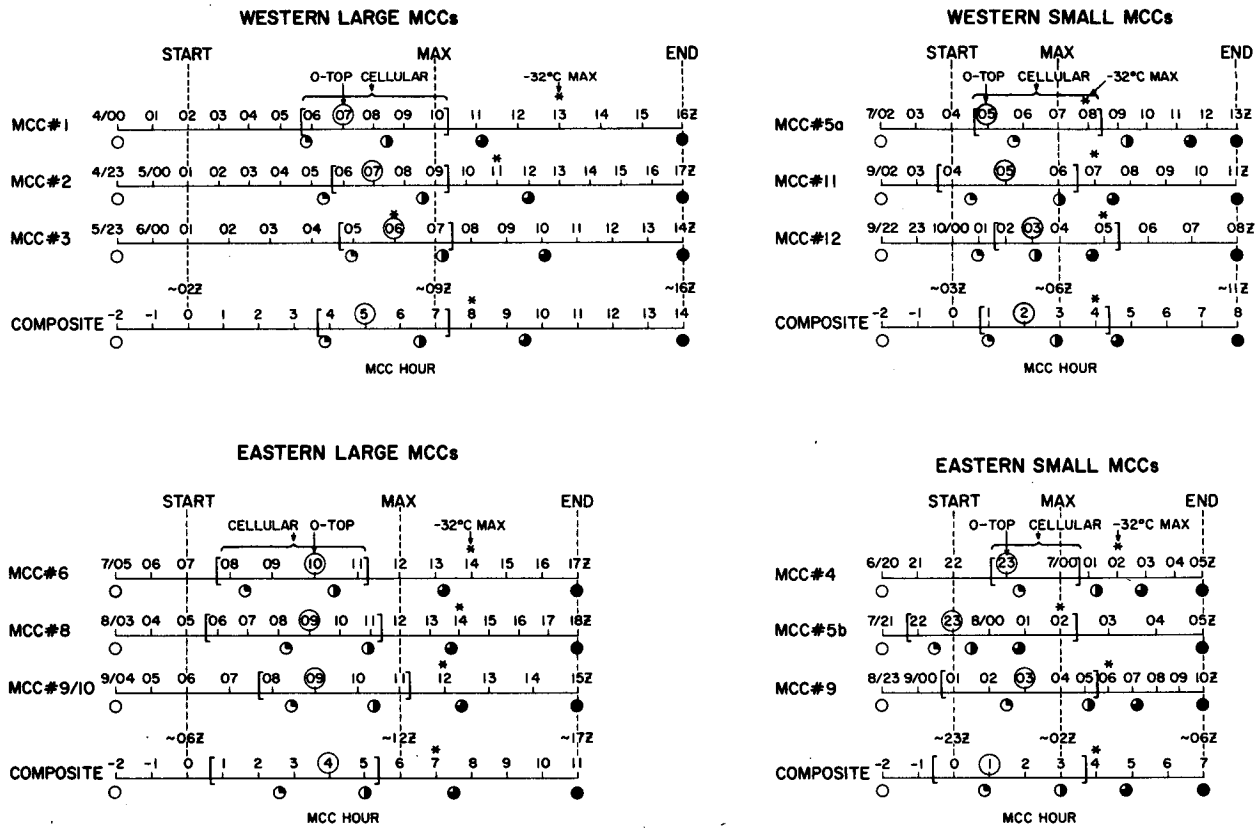

FIG. 4. Stratification of 12 MCCs into four composite categories by geographical genesis region and maximum anvil size. Each MCC is represented by a time scale labelled in GMT hours and is fitted to its composite time scale according to the IR-defined characteristics (defined in text) of "start", "maximum" and "end" (vertical dashed lines). Also indicated are the times of other IR-defined characteristics: a meso-α-scale "cellular" stage (in brackets); an "overshooting-top maximum" (circled); and the maximum size of the −32°C IR area (asterisk). Based on a total accumulated hourly rainfall volume from 2 h prior to "start" to "end", the timing of the total's quartiles is indicated by the appropriately shaded circles under each MCC time scale. The composite MCC for each category, labeled with an hourly time scale "starting" at hour 0, is based on the average timing and durations of these IR and precipitation characteristics for the three individual MCCs. The timing of the composite IR features is rounded to the nearest whole MCC hour.

tation envelopes, where their boundaries were drawn approximately equidistant between stations reporting measurable rainfall and those reporting none (see examples in Fig. 3). An envelope was considered to be associated with the MCC if it was contiguous with the −32°C IR area at either the beginning or end of the hourly period. The area of each envelope was then measured with a planimeter, and all rainfall values within it were arithmetically averaged to give a mean depth. A rainfall volume for each envelope was computed as the product of the area and mean depth (see examples in Fig. 3). For each hour of an individual MCC, multiple envelopes were combined to give a total hourly precipitation area (A) and volume (V). To reduce some of the temporal variability in these values, a 1–2–1 filter was applied, in which the values from the previous, current, and following hours were weighted by 25, 50 and 25%, respectively.

The composite analysis approach to this quantified precipitation information is illustrated in Fig. 4, where the timing of the IR-defined life-cycle characteristics is indicated along an hourly time axis for each MCC. In each composite category, the three individual MCCs are considered to have common composite times of "start", "maximum" and "end". Besides the similarities in genesis region, maximum IR area and mature duration (Table 1), the MCCs in each category were reasonably consistent in terms of other IR-defined characteristics. These include: the durations of "start-to-maximum" and "maximum-to-end"; the timing and duration of the meso-α "cellular" appearance within the "start-maximum-end" sequence; the timing of the "overshooting-top maximum"; the timing of the maximum −32°C IR area; and the absolute GMT times of these IR features. Thus, a realistic time scale for a composite MCC can be derived for each category. The composite's "start" is defined to occur at MCC hour 0, and its "maximum" and "end" are determined by the average "start-to-maximum" and average mature durations, respectively, rounded to the nearest hour. The other composite life-cycle points are similarly determined to the nearest hour.

The averaging methodology for deriving the composite MCC precipitation characteristics is based on

these time scales. Each individual MCC's smoothed hourly values of rainfall area and volume, A and V, were first fitted directly or by linear interpolation onto its composite time scale, with the end of each hourly precipitation period coinciding with the IR-defined MCC hour. For each MCC category, the three individual composite fits were then arithmetically averaged hour-by-hour to give average areas ($\bar{A}$) and volumes ($\bar{V}$). Average hourly rainfall intensities were finally computed as $\bar{R} = \bar{V}/\bar{A}$. Composite histories of the −53° and −32°C IR areas were derived using the same averaging methodology, omitting the 1–2–1 smoothing.

To provide more insight into the average hourly precipitation rates, a similar composite approach was followed in deriving frequency distributions of measurable rainfall reports over various intensity categories. This analysis was carried out separately for the 2.5-mm and 0.25-mm gages, thus providing two independent analyses for each composite. The procedure consisted of tabulating hour-by-hour the number of MCC-related reports exceeding each intensity threshold in each MCC, smoothing these frequencies with a 1–2–1 running average, fitting the smoothed frequencies onto the composite time scale, and summing the three individual-MCC frequencies in each composite. Relative frequency distributions were then calculated by dividing the number of reports exceeding each intensity threshold by the total sample size (the number of measurable reports).

For comparison, a similar analysis was performed utilizing hourly mappings of Manually Digitized Radar (MDR) data, derived from the NWS WSR-57 radar network (Moore et al., 1974). These data consisted of a grid of boxes, each being approximately 84-km square and assigned a code value according to the criteria in Table 2. The frequencies of nonzero MDR values associated with each MCC were tabulated, smoothed and composited in a manner analogous to the rainfall intensities.

d. *Surface data and analysis*

In the case studies of MCC evolution in section 4, the roles of significant surface features such as fronts, troughs and mesoscale outflows from convective activity are qualitatively described. The identification of their existence, movements and roles has required the detailed analysis of extended sequences of hourly surface maps, augmented by IR and visible satellite imagery. The surface analyses are based on all available (first and lesser-order) hourly surface observations (cloud reports and comments included) on file with the Bureau of Reclamation. For the sake of brevity, we present only one surface analysis near the beginning of each case.

4. The meso-β-scale substructure and evolution of the MCCs

Several meso-β-scale characteristics of MCC evolution are described qualitatively in this section. In order to emphasize the similarities and differences from case to case, we first describe each western large system and one eastern large system from Table 1. A general discussion of the episode's MCC substructural variability follows in section 4e.

a. *MCC number 1—Western system of 3–4 August*

The first MCC of the episode (MCC number 1 from Fig. 1) developed from afternoon convection on the High Plains of western Nebraska and northeast Colorado, moved eastward through the night of 3–4 August, and weakened in the early daylight hours over the Mississippi Valley (Fig. 2). At the system's formative stage at 0000 GMT 4 August, an upper air analysis (Fig. 5a) depicts several notable low to midtropospheric features that are consistent with previous MCC studies (Maddox, 1983; Bosart and Sanders, 1981; Maddox and Doswell, 1982; Cotton et al., 1983; Wetzel et al., 1983). These include: 1) a pronounced southerly low-level jet from the Texas panhandle into western Kansas and Nebraska; 2) pronounced lower-tropospheric warm advection (from the elevated heat source over the southern Rocky Mountain plateau) from 850 to 700 mb in the same region; 3) and abundant moisture (exceeding 30 mm of precipitable water) to the south and east of the developing system. The shaded region of

TABLE 2. Manually digitized radar (MDR) data code.

Code	Coverage in box	Maximum reflectivity (dBZ)	Maximum convective rainfall rate (mm/h)	Category
0	No echo	N/A	0	
1	Any VIP1	<30	0–5	light
2	≤½ VIP2	30–40	6–27	moderate
3	>½ VIP2			
4	≤½ VIP3	41–45	28–55	heavy
5	>½ VIP3			
6	≤½ VIP3, 4	46–49	56–114	very heavy
7	>½ VIP3, 4			
8	≤½ VIP3, 4, 5, 6	50–56 or	115–180	intense or
9	>½ VIP3, 4, 5, 6	>56	>180	extreme

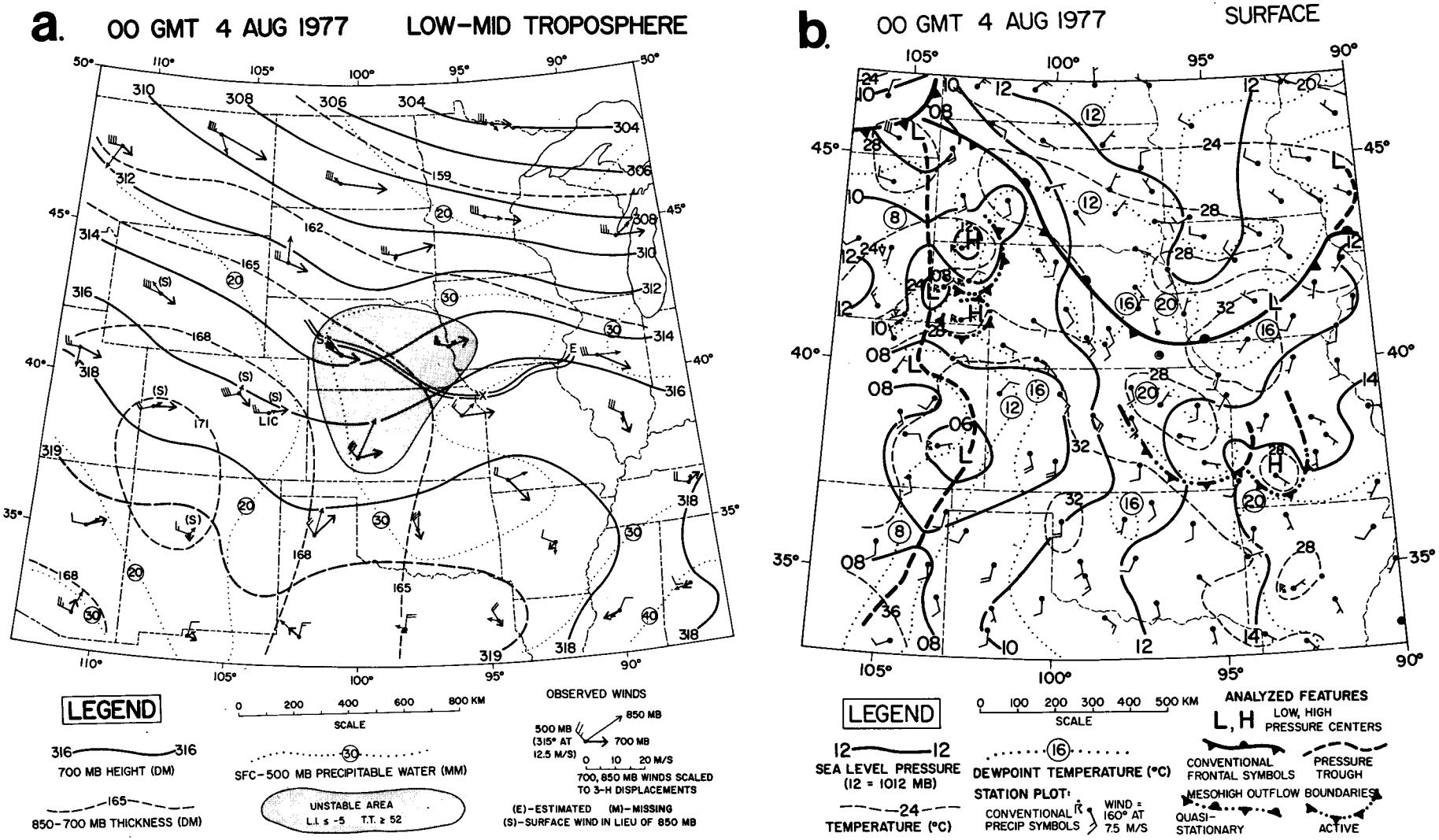

FIG. 5. Synoptic conditions at 0000 GMT 4 Aug 1977, near the development time of the western MCC number 1 (refer to legends in figure for analysis and plotting conventions). (a) Low to midtropospheric features. Analyzed fields include 700-mb heights, 850 to 700-mb thicknesses and surface to 500-mb precipitable water. Shaded region highlights area of most pronounced latent instability, based on lifted index (L.I.) and total-totals index (T.T.) [Miller, 1972]. Winds at 850, 700 and 500 mb are plotted at conventional rawinsonde sites (unlabelled) and at Limon, CO (LIC). The track of the −53°C IR area centroid over the period indicated by the time line in Fig. 4 is given by the double line, with the "start", "maximum" and "end" positions denoted as S, X and E, respectively. (b) Surface features. Analyzed fields include sea level pressure, temperature and dewpoint temperature. Winds and precipitation symbols are plotted at observation sites. Analyzed meteorological features are described in the figure legend.

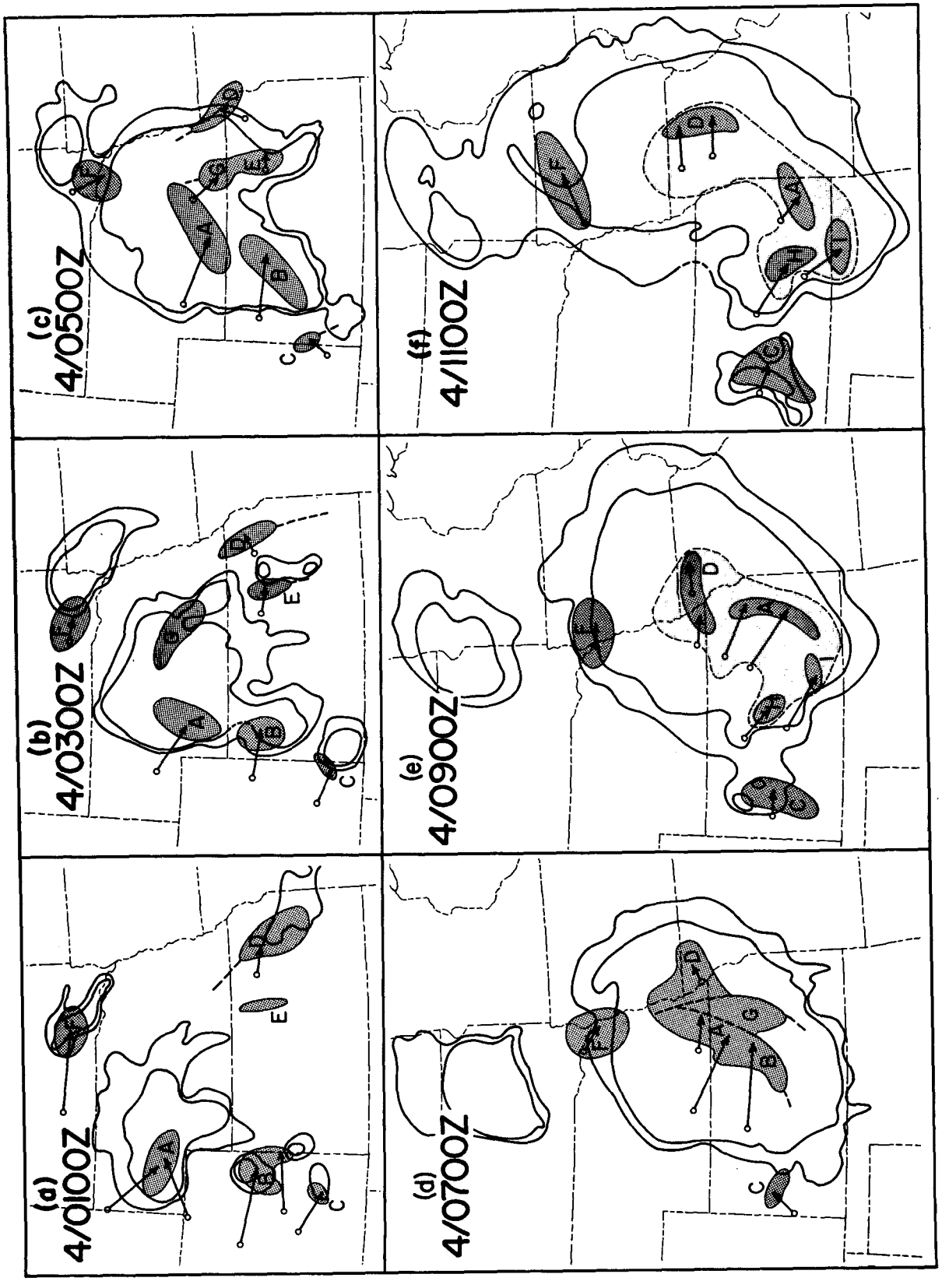

FIG. 6. Schematic IR satellite and radar analysis at 2-h intervals, from 0100 to 1100 GMT 4 Aug 1977, for the western MCC number 1. The anvil cloud shields are indicated by the −32° and −53°C IR contours (outer and inner solid lines, respectively), remapped from satellite images at the labeled times. Darkly shaded regions (identified by letters) denote significant radar-observed, meso-β-scale convective features at about 25 min after the indicated whole hour, with the vectors showing their previous 2-h movements. The dashed line segments extending from the meso-β convective features indicate flanking axes of weaker convection. In the more developed MCC stages, in (e) and (f), the light-shaded area within the dashed envelope indicates weaker, more uniform and widespread echo.

pronounced latent instability over Nebraska and Kansas corresponds closely to the center of subsequent MCC development.

At 700 mb, a weak short wave extended across the development region from South Dakota to eastern New Mexico, with a downstream ridge from northeastern Texas into Missouri and Iowa. The 500-mb height field (not shown) indicates no short-wave feature in the area. However, objective kinematic analysis (not shown) of the depicted 500-mb winds indicates a region of cyclonic vorticity advection (CVA) centered over northeastern Colorado, upstream of an anticyclonic vorticity axis running roughly along the eastern border of Colorado into northeastern New Mexico. Thus, the developing meso-α-scale cloud system in Fig. 2a, occurring at the leading edge of this CVA field, was apparently supported dynamically at midlevels in a manner consistent with the development of the composite MCC as described by Maddox (1983).

Surface features at the same time (Fig. 5b) included a north/south (N/S) leeside trough that had existed all afternoon along the High Plains from Montana to New Mexico, and a weak stationary front extending NW–SE across eastern Nebraska. The southeasterly wind in the moist tongue (dewpoint temperatures >16°C) to the southwest of this front provided low-level moisture to the developing convection in western Nebraska, which produced the expanding complex of mesohighs.

The schematic IR satellite and meso-β radar analysis in Fig. 6 illustrates the important evolutionary features of MCC number 1. At 0100 GMT (Fig. 6a), three meso-β convective clusters (labelled A, B and C) were aligned N/S in western Nebraska and eastern Colorado. These originated along the Wyoming and Colorado foothills and are typical of the eastward-tracking orogenic[6] convection induced by the differential diurnal heating over the mountains and plains (Wallace, 1975; Paegle, 1978). In this case, the climatological afternoon upslope wind produced by this diurnal forcing over the High Plains (Toth and Johnson, 1985) was further enhanced by the synoptic pressure gradient to the north of the low in eastern Colorado (Fig. 5b). Cluster A formed earliest and was most intense, producing severe winds and large hail in western Nebraska.[7] Moving into the moist tongue seen in Fig. 5b, cluster A intensified most rapidly and produced the bulk of the cold cloud shield which met MCC criteria by 0200 GMT.

This N/S axis of clusters continued to move east over the next several hours (Fig. 6a–d), with clusters A and B moving particularly fast on convergent tracks and becoming organized into meso-β squall lines by 0500 GMT (Fig. 6c). Their convergent tracking tendency was perhaps due in part to steering by the confluent 700-mb flow in this region, and their squall-line organization was likely due to their moving into the low-level jet region, thereby increasing the low to mid-tropospheric shear (see Fig. 5a). The 0500 GMT IR image (Fig. 2c) identifies these clusters as distinct bands of overshooting cumulonimbi.

A second major axis of meso-β convective activity that was important in the MCC's evolution developed in a NW/SE orientation in eastern Kansas and Nebraska. In northeastern Kansas, cluster D (Fig. 6a) was a residual area of weak convection that had moved from south-central Nebraska through the day and produced the surface mesohigh in eastern Kansas (Fig. 5b). The 0000 GMT IR image (Fig. 2a) shows an enhanced cloud shield associated with D, its axis of residual cloudiness extending northwestward into Nebraska, and a thin, unenhanced cloud line along the western boundary of the mesohigh. The latter feature developed into the meso-β convective band E by 0100 GMT (Fig. 6a). By 03 GMT (Fig. 6b), cluster G developed along the residual cloud axis to the northwest of D, parallel to the surface front in Nebraska.

We note qualitatively that the most intense phase of MCC development, between 0300 and 0700 GMT (Figs. 6, 2), was focused near the intersection of this loosely-defined NW/SE axis of convective clusters (G–E) in eastern Nebraska and Kansas, as it was overtaken from the west by the faster-moving N/S axis A–B. By 0500 GMT (Figs. 6c, 2c), the western portion of G was overtaken as it merged into the northeast end of A. The eastern portion of G rapidly intensified as a right-moving severe storm that produced a 50-km hail swath (and its own overshooting top signature) and merged with the meso-β band *E*. Over the next 2 h, clusters A and B continued on their fast, convergent tracks, so that by 0700 GMT (Fig. 6d), they had merged and overtaken clusters G and E, creating a large meso-β (or small meso-α) band of intense convection. Cluster D lost much of its discrete identity and expanded as an echo of more uniform intensity that merged into the A–B–G band. This complex produced the MCC's "overshooting-top maximum" at about this time (Fig. 2d). A tornado and a 200-km track of severe surface winds were produced by cluster A during the merging of these features, qualifying this case as a "derecho" (Johns and Hirt, 1983).

Analogous intersecting meso-α-scale linear features are seen to play key roles in the next two western large MCCs subsequently described. In the most general terms, meso-β convective features originate along (and subsequently help define) the meso-α axes, and those meso-β features nearest the point of intersection of the meso-α axes (in this case clusters A and G) intensify

[6] Following Bergeron (1968), we introduce *orogenic*, literally meaning "produced by mountains," as a more precise replacement for *orographic*, literally meaning "describing mountains." We have retained the familiar form of the root *oro-* instead of the one used by Bergeron, *ore-*: their meanings are identical.

[7] These and subsequent severe weather events are extracted from "Storm Data", published monthly by the National Climatic Data Center, NOAA/NESDIS, Asheville, NC 28801.

most rapidly, sometimes merge, and become the apparent core of the MCC.

After the merging of the discrete meso-β features into a larger meso-β cluster of widespread intense reflectivity (Fig. 6d), a larger area of more uniform and weaker echo developed (Fig. 6e). The meso-β convective band A continued its southeastward motion near the leading edge of this larger precipitation field, so that the echo structure of the MCC resembled that of tropical cloud clusters (Zipser, 1977; Leary and Houze, 1979). The other meso-β convective features became weaker and/or ill-defined within the larger precipitation field, and new meso-β features (H, I) developed on the southwestern flank of the field.

Whereas until the "overshooting-top maximum" (Fig. 2d) the movement of meso-β convective features displayed a convergent tendency (Fig. 6a–d), in the weakening stages the tracks became divergent, with the northern bands (F, D) moving eastward and the southern ones (A, I, H) southeastward (Fig. 6e, f). This divergent tracking may be due to further convective growth being forced at the boundary of the expanding surface mesohigh.

b. MCC number 2—Western system of 4–5 August

Cotton et al. (1983) describe the next evening's MCC (number 2 from Fig. 1) from its convective roots over the Colorado Rockies through its up-scale growth over eastern Colorado. Its continued evolution across Kansas is followed by Wetzel et al. (1983). Here we highlight its similarities to, as well as its significant differences from, MCC number 1.

Low to midtropospheric features at the system's formative stage at 0000 GMT 5 August (Fig. 7a) were similar to those seen in the first case. However, a cool surge of northerly flow over the northern plains (see 850-mb winds) resulted in the most unstable region (shaded area) being further south than on the previous evening, along with a similar southward displacement of the low-level jet and positive thickness advection (compare with Fig. 5a). These factors likely contributed to the more southern track of MCC number 2 across the western plains.

Important surface features at 0000 GMT (Fig. 7b) included: a complex of mesohighs in eastern Colorado, produced by afternoon orogenic convection; a weak front, associated with the cool surge mentioned above and extending east-northeastward from its stalled position in eastern Colorado; and an E/W thermal, moisture and wind discontinuity across southern Kansas. This latter feature was the remnant of the outflow boundary produced by the previous evening's MCC, and it also closely marked the southern extent of that system's rainfall.

As on the previous day, the IR/radar analysis shows that the orogenic convection became organized into a N/S string of meso-β convective clusters and moved coherently eastward (clusters A, B and C in Fig. 8a, b). With strong easterly moisture advection in western Kansas (Fig. 7b), clusters A and B persisted as intense MCC components (B produced severe winds and hail in eastern Colorado), while C, to the south of this moist inflow, remained a relatively weak peripheral cluster on the southwest flank of the MCC.

Though convection farther east tended to develop in meso-β bands oriented E/W, its evolution was more chaotic and its movement less coherent than the N/S string of orogenic clusters. Cluster F, for example, developed in northeastern Kansas as a relatively independent and stationery mesoscale convective system of sub-MCC dimensions, producing its own intense cloud shield that persisted through 10 GMT as a somewhat detached lobe of the main MCC (Fig. 8b–e). Cluster D, on the other hand, was apparently triggered along the surface discontinuity in southern Kansas (Fig. 8a, b), then displayed a general northward movement (Fig. 8c, d) due to widespread cell growth (dissipation) on its north (south) side. Associated with this northward movement was the dissipation of the initial E/W IR shield produced by D in southern Kansas (Fig. 8c) and the filling in of the meso-α cloud shield between clusters A–B and F (Fig. 8d).

The core of the MCC during its intense up-scale growth centered on the eastward-moving N/S axis of clusters (A–B) as it overtook the less organized activity further east. From 0300–0500 GMT, IR imagery indicates two distict centers of intense convection, located near the intersections of the N/S axis with the E/W-oriented surface front in northwestern Kansas (cluster A) and with the old outflow boundary in southwestern Kansas (cluster B). After 0500 GMT, the coldest cloud-tops consolidated between these two centers of activity into a larger region of overshooting convection, becoming the apparent core of the intense MCC and persisting through 0700 GMT (Fig. 8c, d). The convergent tracking of clusters A and B over the previous several hours, again influenced by confluent 700-mb flow (seen from Nebraska to the Texas panhandle in Fig. 7a), was perhaps important to this consolidation.

After the MCC's "overshooting-top maximum" at about 0700 GMT, the N/S axis lost its identity as clusters A and B weakened considerably. Cluster D continued its northward propagation and became the apparent core of the main MCC, which maintained a highly organized meso-α appearance through 0900 GMT (Fig. 8d, e). By this time, however, two distinct centers of intense overshooting activity again became apparent, associated with the now divergently tracking clusters D and B (Fig. 8e). Comparing Figs. 8d–e and 6d–e, a distinct difference between the two systems is that the major meso-β components of MCC number 2 did not become as cohesively unified towards a meso-α organization as in MCC number 1.

During the decaying stages of the MCC (after the maximum −53°C IR area), cluster D weakened and

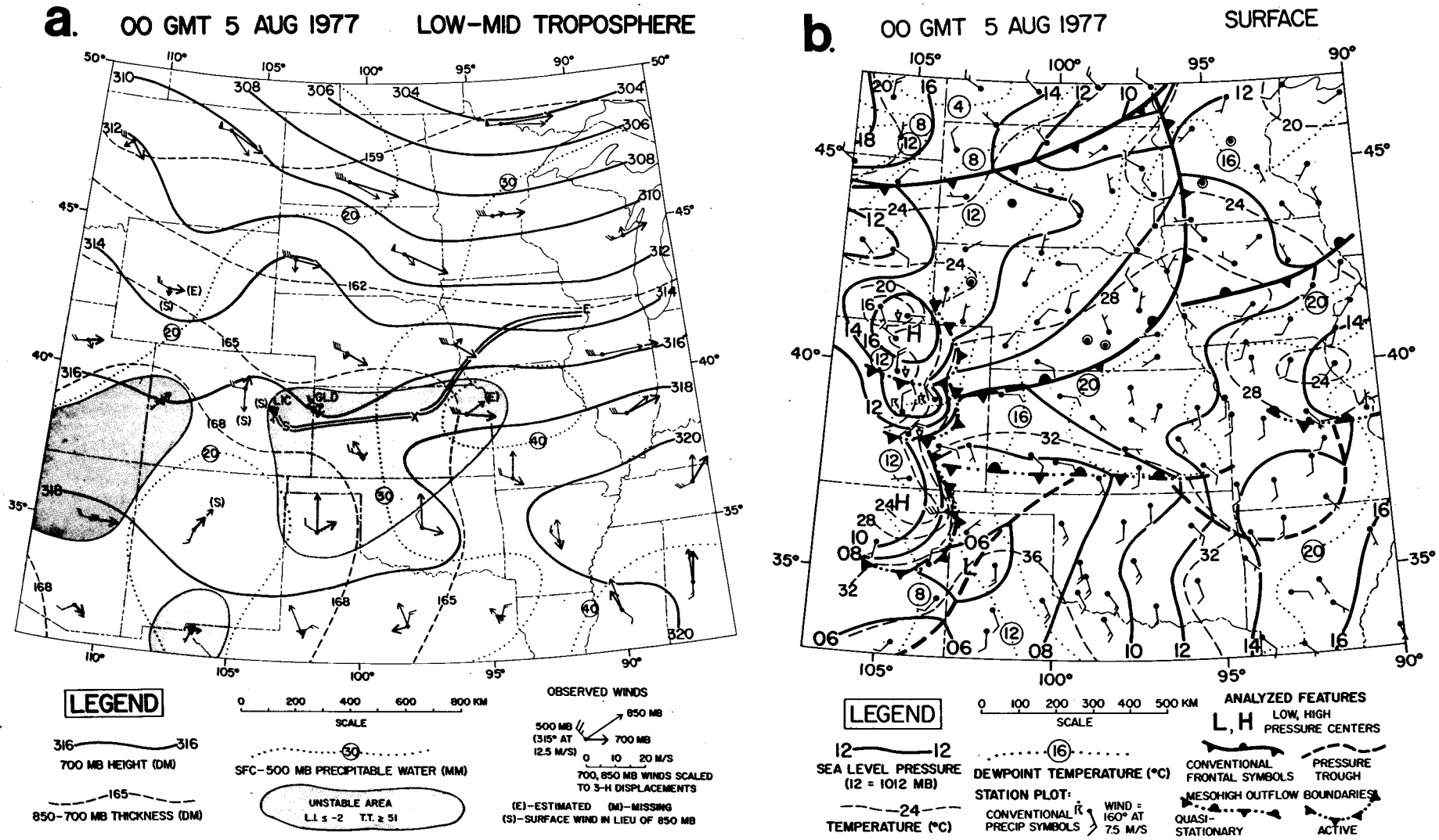

FIG. 7. Synoptic analysis at 0000 GMT 5 Aug 1977, near the development time of the western MCC number 2. (a) Low to midtropospheric features and the storm track are as in Fig. 5a. An additional sounding was available at Goodland, KS (GLD). (b) Surface features are as in Fig. 5b.

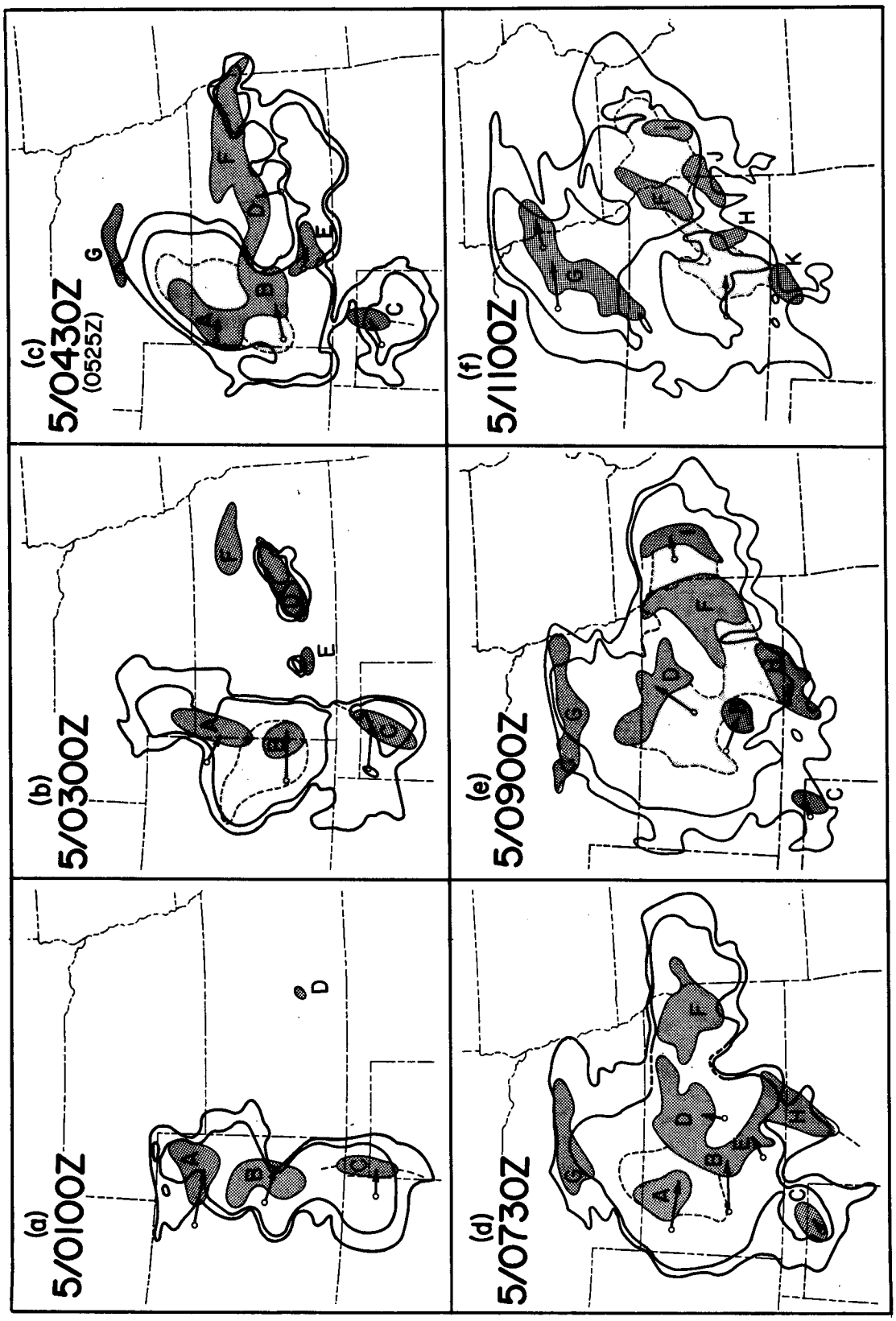

FIG. 8. Schematic IR satellite and radar analysis, from 0100 to 1100 GMT 5 Aug 1977, for the western MCC number 2, similar to Fig. 6. Dashed portions of IR contours [as in northeast Kansas in (d)] are estimated positions when the contours are ill-defined in the imagery. The second time label in (c), 0525 GMT, denotes a radar analysis time differing from the hour of the IR image, 0430 GMT.

merged into the southern end of G, which had been a minor peripheral component on the northern edge of the MCC in Nebraska. Previously stationary, cluster G now assumed a NE/SW orientation and began to move eastward (Fig. 8e, f), where it intensified and produced much precipitation for several more hours over Iowa. The development and maintenance of this NE/SW band was apparently linked to the approach from the northwest of a surface cold front, seen in South Dakota at 0000 GMT (Fig. 7b). The other meso-β convective components weakened during the MCC's decay and became organized in a similarly oriented NE/SW line across eastern Kansas and northern Missouri, loosely joined by a decaying shield of "anvil" precipitation. Divergent movement between the meso-β components was evident in the decaying stage, though not as pronounced as in the previous evening's MCC.

c. *MCC number 3—Western system of 5–6 August*

The next evening's system (number 3 from Fig. 1) became the final large, well-organized High Plains MCC of the episode, with the subsequent western systems over the next five days being smaller and/or attaining a less-organized meso-α "cellular" stage. The synoptic conditions at 0000 GMT 6 August were similar to the previous two cases. A stronger cool surge over the northern plains than on the previous evening is evident aloft by lower 850–700 mb thickness values (Fig. 9a), and at the surface by a cold front that had advanced well into Kansas (Fig. 9b).

Pre-MCC precipitation activity was much more widespread than in the previous cases. Postfrontal rain and rainshowers were scattered across Nebraska, and eastward-propagating convection had developed early in the day over the eastern slopes of Colorado. By 0000 GMT this orogenic convection had become widespread over the Colorado and New Mexico High Plains, producing a growing complex of mesohigh outflows (Fig. 9b).

The IR/radar analysis in Fig. 10a illustrates the meso-β organization of convection at around 22 GMT. Clusters A, B and C (and a recently dissipated cluster ahead of A) formed over the foothills early in the day, moved onto the plains around midday, and by this time were nearing the Kansas border. Another series of orogenic convective clusters (G, H and I) formed a second distinct N/S line about 3 h behind the first. Ahead of these N/S axes of convection, clusters D, E and F originated after 2000 GMT as relatively weak convection (no cold IR cloud shield) and were arranged in a SW/NE orientation that was parallel to and on the north side of the cold front.

As on the previous evenings, the intersection of the eastward-moving axis of orogenic convection (A–B–C) with the more E/W-oriented axis (D–E–F) marked the location of intense MCC development. In this case, cluster B weakened and dissipated as it approached clusters F and E, which simultaneously intensified (Fig. 10a, b). Cluster F produced large hail in western Kansas for over 2 h along with some tornadic activity, and cluster E merged into the intensifying southwest end of the stationary convective band D (Fig. 10b, c).

Even though the MCC reached mature IR dimensions by about 0100 GMT, satellite data at 0200 GMT (Fig. 10c) indicate that the "meso-α" complex was actually composed of three distinct regions of mesoscale convective organization: clusters F and D, which produced the primary, intensifying anvil in Kansas; the anvil lobe to the southwest that was produced by the meso-β features C, I and J; and an intense anvil lobe in eastern Colorado produced by the second series of orogenic convection. The latter two anvil lobes subsequently weakened in convective intensity, while clusters F and D grew and merged to form a large band of intense convection across central Kansas (Fig. 10d). This merger produced a "bow-echo" radar pattern (Fujita, 1981) and severe weather over central Kansas at the center of the consolidated convective band. The persistence of this NE/SW band was apparently due in part to the active cold front across Kansas (Fig. 9b). Such control by a cold front on the meso-β-scale organization of convection is similar to what was seen in the decaying stage of MCC number 2 the previous night.

After the MCC reached its "overshooting-top maximum" (0600 GMT) and its largest −53°C IR areal extent (0700 GMT), the convective activity of the system was dominated by cluster L in northern Missouri (Fig. 10f). This feature originated ahead of the MCC hours earlier, and was one of several meso-β convective features strung eastward from Missouri along the E/W outflow boundary of the weakened system number 2 (Fig. 9b). As the MCC (and the cold front) approached Missouri, cluster L rapidly intensified, first becoming an intense anvil lobe on the MCC's eastern flank, and then becoming the core of the system (Fig. 10d–f). This gave the appearance of discrete propagation of the MCC on the meso-β scale, resulting from the weakening of the older meso-β convective features in Kansas and the simultaneous development of newer convection (L) at the intersection of the system with the E/W discontinuity. Following 0800 GMT, cluster L evolved into a larger, more stratiform precipitation feature that dominated the MCC through its decay over northern Illinois. A secondary, peripheral convective band (M) developed from previously unorganized shower activity over Nebraska during this decay period.

d. *MCC number 6—Eastern system of 6–7 August*

A large MCC formed on each of the next three evenings over the lower, more level eastern genesis region of Iowa and Missouri (see Fig. 1). The first, MCC number 6, is highlighted in this section in order to compare it with the western systems.

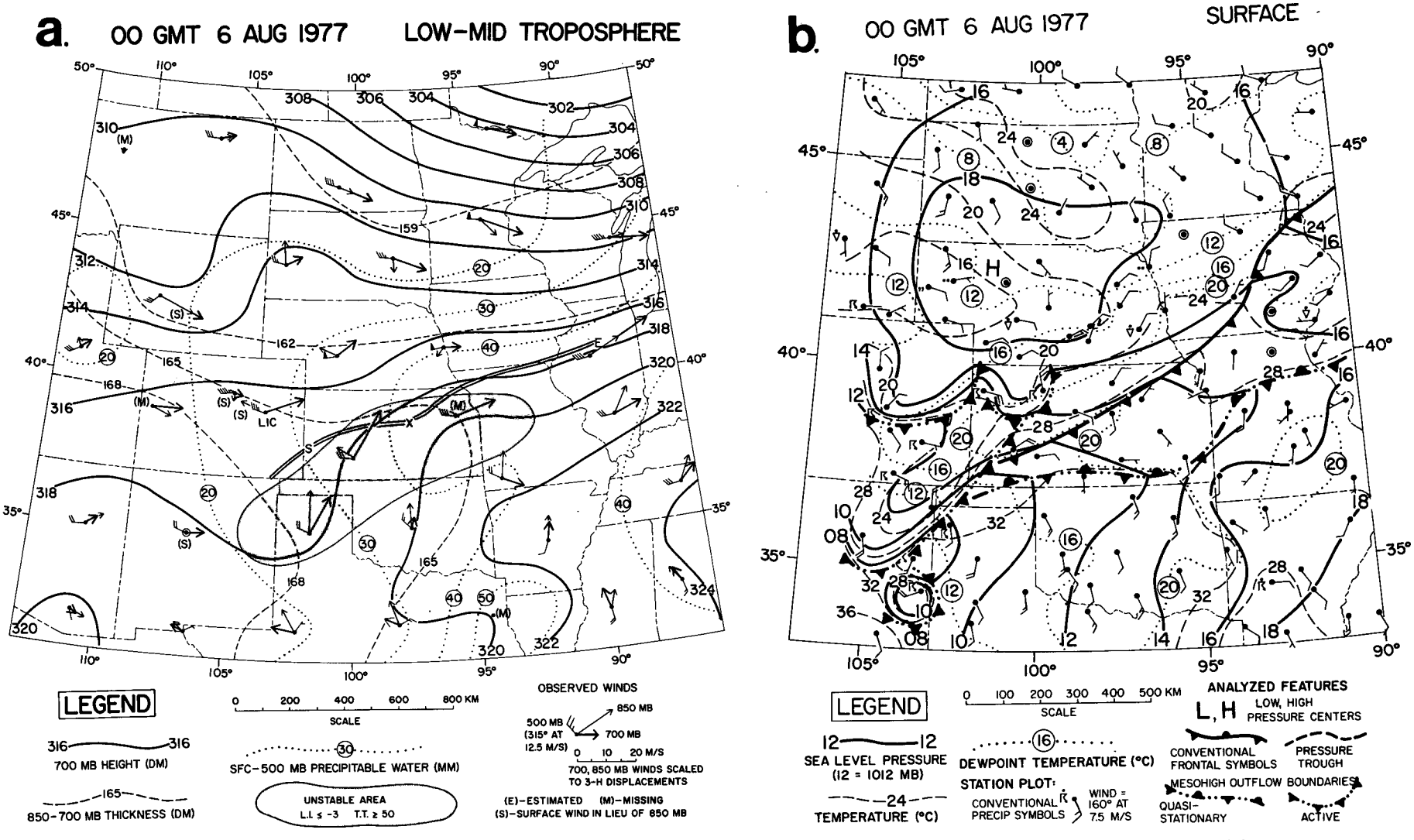

FIG. 9. Synoptic analysis at 0000 GMT 6 Aug 1977, near the development time of the western MCC number 3. (a) Low to midtropospheric features and the storm track are as in Fig. 5a. (b) Surface features are as in Fig. 5b.

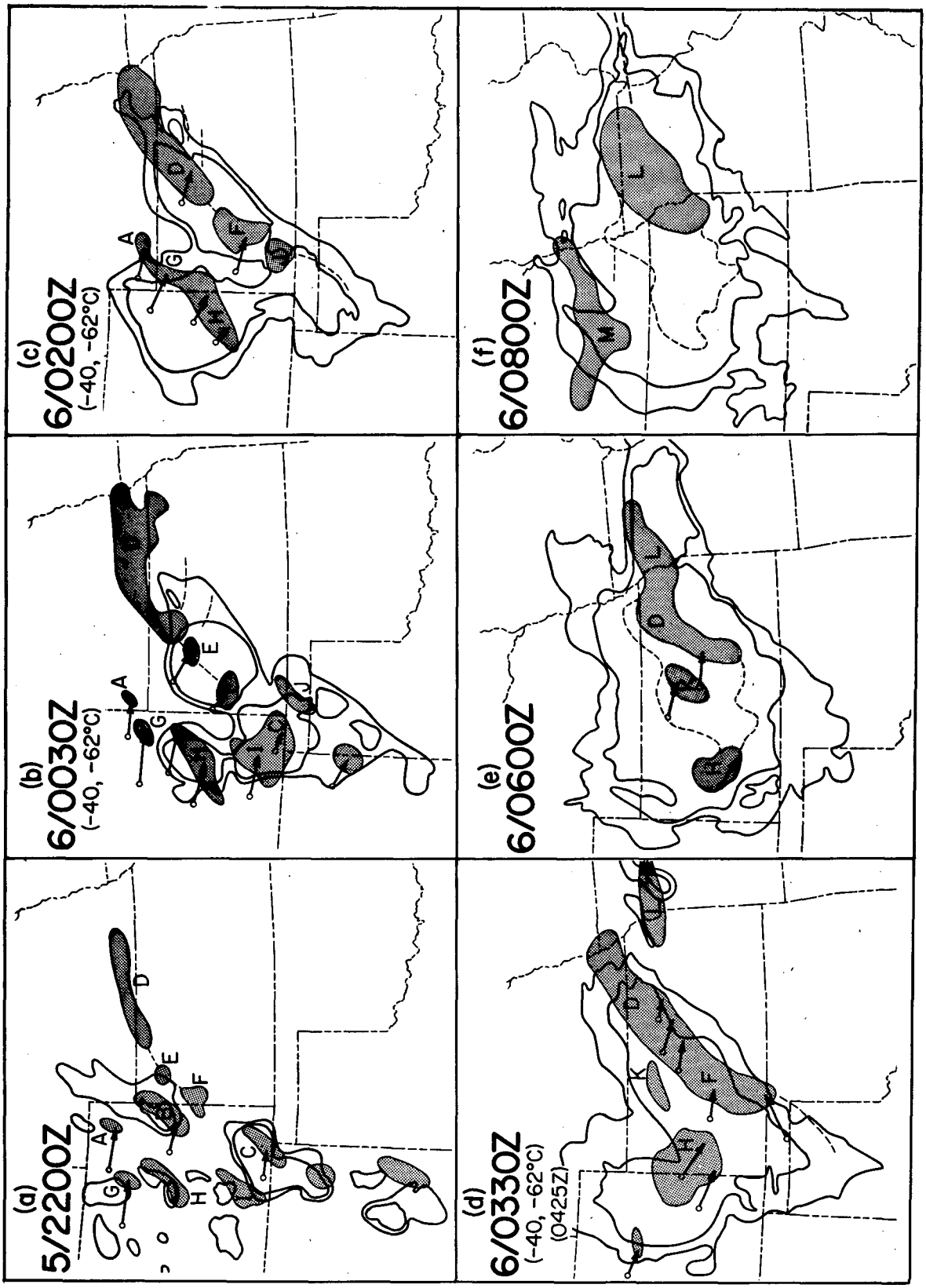

FIG. 10. Schematic IR satellite and radar analysis, from 2200 GMT 5 Aug to 0800 GMT 6 Aug 1977, for the western MCC number 3, similar to Figs. 6 and 8. The second time label in (d) denotes a radar analysis time differing from the hour of the IR image. In (b), (c) and (d) the IR contours are −40° and −62°C.

The low to midtropospheric features at 0000 GMT 7 August, several hours before the system's development, are shown in Fig. 11a. The genesis region of southern Iowa was under stronger flow aloft, and with a stronger short wave to the north, than in the previous cases. Whereas the southerly low-level jet in the western cases terminated in the High Plains genesis regions, in this case it curved anticyclonically over Kansas and continued as a southwesterly jet through Illinois. Strong warm advection from 850 to 700 mb also extended further east.

The first thunderstorms associated with MCC number 6 developed at about 0300 GMT in northwestern Missouri. As indicated on the surface analysis for that time in Fig. 11b, this development was near the intersection of two meso-α discontinuities. One of these was the cold front which strongly influenced MCC number 3 the evening before (see Fig. 9b), and which by now was stationary in a ENE/WSW orientation across Kansas and southern Iowa. The second boundary, extending southeastward across Missouri into southern Illinois and Indiana, was produced and maintained by the small but intense eastern MCC number 4, which developed in northern Missouri several hours earlier and by now was weakening over Indiana.

As the small MCC number 4 matured near 2200 GMT, it produced a concentrated outbreak of severe weather, including numerous tornadoes, along a 100-km track in central Illinois. This outbreak is described in detail by Forbes and Wakimoto (1978; 1983). As they indicate in the former reference, MCC number 4 developed near the intersection of an E/W discontinuity that formed along the southern extent of the precipitation produced by MCC number 3, with a NE/SW axis of residual cloudiness trailing from that same system. Thus, the meso-α boundary in Fig. 11b was actually a preexisting feature that was reinforced by MCC number 4.

The warm sector to the south of the intersecting meso-α boundaries was characterized by strong southerly flow feeding warm, moist air towards the intersection. This configuration of surface discontinuities in the MCC's genesis region was closely repeated for the second and third large eastern MCCs during the next two evenings.

The MCC's evolution is illustrated by the IR/radar analysis (augmented by hourly rainfall areas) in Fig. 12. By 0430 GMT (Fig. 12a), the initial thunderstorm activity in northwestern Missouri consolidated into three small meso-β clusters (A, B and C) and produced a small, convectively intense anvil cloud. Meso-β feature D in northern Iowa was a less intense band of thunderstorms on the north side of the stationary front and remained a minor component of the MCC. In the wake of MCC number 4, now weakening over Indiana and Ohio, meso-β cluster E in central Illinois was also a relatively weak, recently formed feature.

Over the next 2 h, clusters A, B and C consolidated into a larger intense cluster (A) on the western flank of the rapidly expanding anvil cloud (Fig. 12b). A new meso-β band, F, formed to the northeast of cluster A and began developing southeastward into the northwestward expanding band E. Satellite images show that this NW/SE oriented band E–F developed within a thickening band of cloudiness that was advecting northeastward from its origins several hours earlier along the weak outflow boundary in Missouri. This convection produced an anvil lobe protruding southeastward from the initial anvil.

The MCC's anvil had an intense, meso-α "cellular" appearance from about 0800 to 1100 GMT (Fig. 12c, d). Though cluster A and the E–F band became aligned into a common, more extensive E/W band, the radar and rainfall data show that the most intense convection persisted as two separate meso-β regions, in southeast Iowa and in central Illinois. Towards the end of this intense MCC phase, a new meso-β cluster, G, formed just to the southeast of cluster A.

As the MCC weakened after 1100 GMT (Fig. 12e, f), cluster G propagated southeastward away from the weakening cluster A, similar to the divergent tracking seen in the western cases. The more interior precipitation feature E expanded into a larger region of relatively light, stratiform rain, with its convective elements concentrated along its southern edge. Cluster E persisted as a large, coherent feature with a southeastward drift through 15 GMT, when it began to break up into weak, divergently tracking elements.

e. Discussion of substructural variability

The most prominent feature of the four large MCCs just described was the tendency for the strong convection to be organized into meso-β-scale convective features, several of which existed simultaneously throughout the life cycle of the meso-α system. It is this multiplicity of meso-β elements, in fact, that distinguished the evolution of the large MCCs from the smaller ones. The small MCCs were generally dominated by a single meso-β convective feature, with the resultant meso-α system having a smaller cloud shield and shorter mature duration and producing much less rainfall than the larger systems (Table 1).

The large systems, because of their multiple meso-β elements, displayed a more complex and variable evolution. Some of this variability could be explained by the configuration of surface fronts, mesoscale outflow boundaries of earlier convective activity, and residual axes of cloudiness extending from earlier convection. Such features were preferred axes for the generation of convection. For the western systems, a N/S string of meso-β convective features developed in diurnally forced (or enhanced) upslope flow, moved eastward, and intensified into the mature MCC as it overtook meso-β activity that developed farther east.

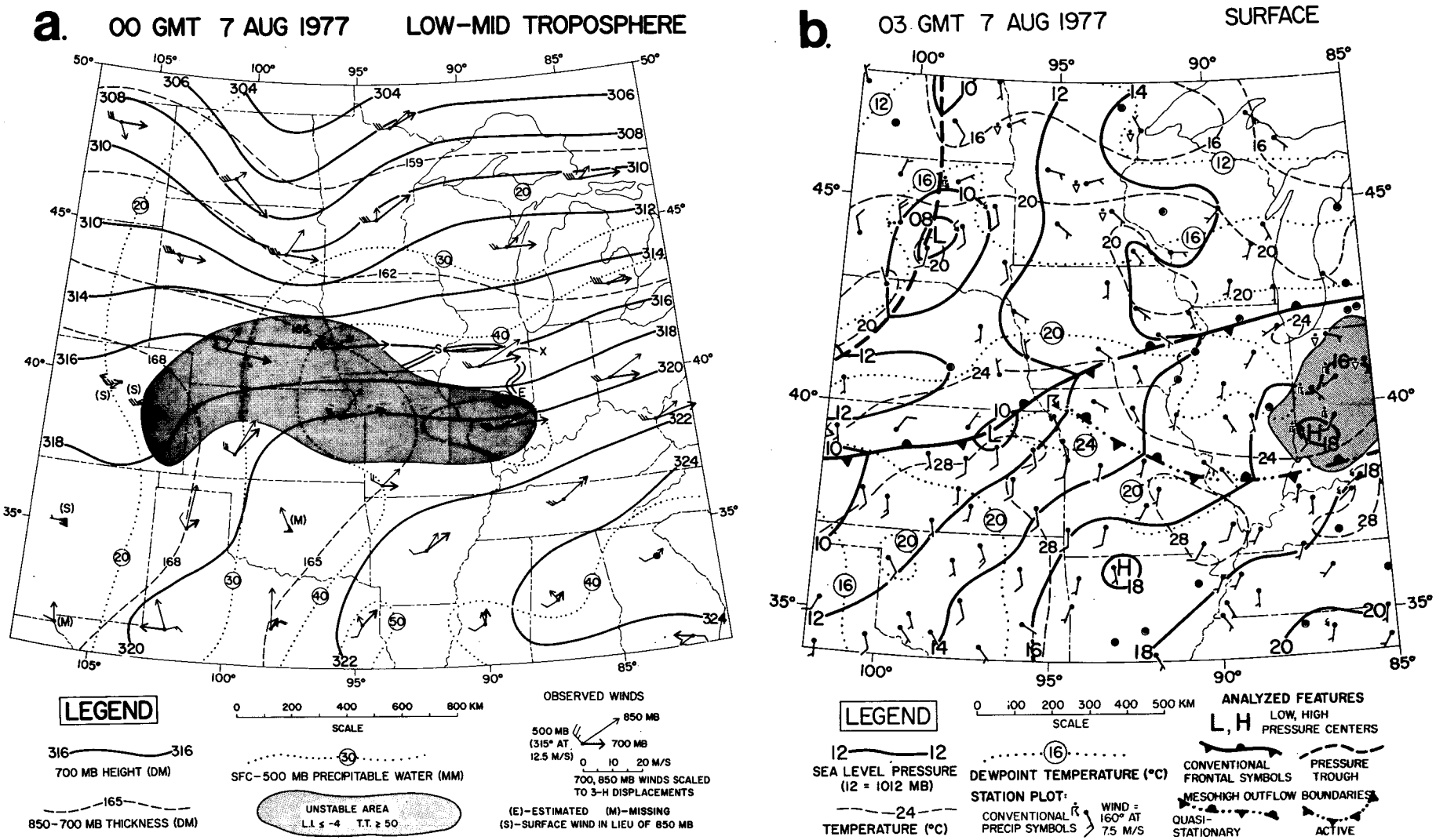

FIG. 11. Synoptic analysis near the development time of the eastern MCC number 6. (a) Low to midtropospheric features at 0000 GMT 7 Aug 1977 and the storm track are as in Fig. 5a. (b) Surface features at 0300 GMT 7 Aug 1977 are as in Fig. 5b. The shaded region over Indiana denotes the −32°C IR cloud shield associated with the small eastern MCC number 4. The large thunderstorm symbol in northwest Missouri denotes the location of initial thunderstorm development for MCC number 6.

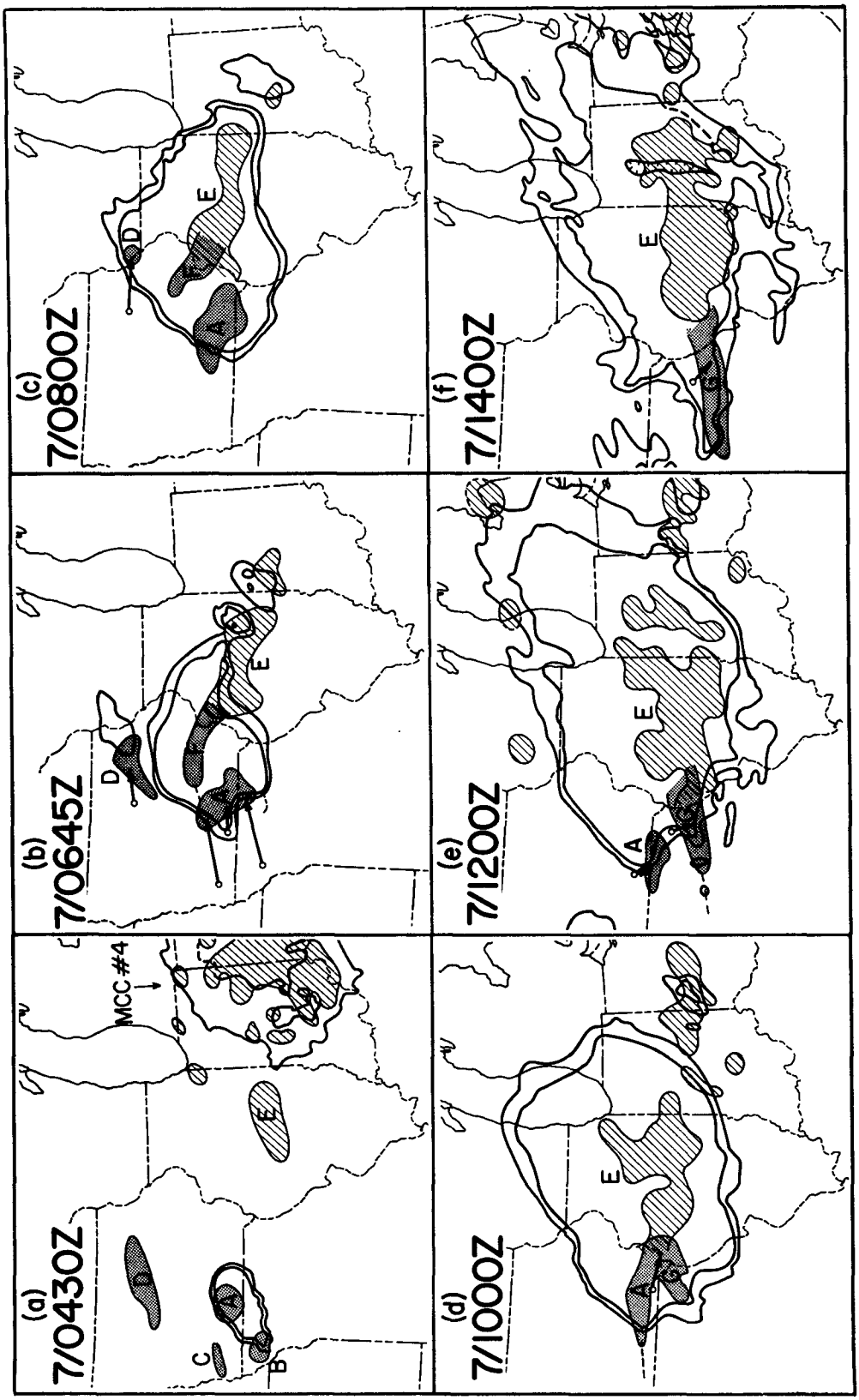

FIG. 12. Schematic IR satellite and radar analysis for the eastern MCC number 6, similar to Figs. 6, 8 and 10. East of the area of reliable radar coverage, hatched envelopes denote regions of measurable precipitation for the hour ending on the whole hour after the indicated IR time.

The eastern MCCs, without such orogenic meso-β components, developed instead near the intersection of a large-scale front and an old, meso-α outflow boundary to its south. Fewer meso-β convective components were involved in the formative stages of the eastern MCCs, which instead tended to grow up-scale more rapidly from one or two vigorous meso-β clusters. A probable contributor to this faster growth was the very moist environment (>40 mm precipitable water), whereas the western MCCs became well organized only after they passed the 30 mm contour (Figs. 5a, 7a, 9a and 11a).

In Fig. 13, the environmental winds accompanying the four MCCs are summarized. Also plotted are the mean velocity of the meso-β convective features (V_β) and the average velocity of the −53°C IR cloud shield (V_α), both computed over the "start-to-maximum" period. These hodographs help explain some of the substructural variability seen between the systems during their growth stage.

For instance, the well-organized squall line structure of the major meso-β components in MCC number 1 (clusters A and B in Fig. 6c–e), as well as its derecho characteristics and faster V_β, may have been due to stronger low to mid-tropospheric shear in that case (4.1 $\times 10^{-3}$ s^{-1} in Fig. 13a). While the relation between shear and convective organization and movement is not clear, there is observational and modeling evidence that increasing shear aids the development and maintenance of relatively fast-moving squall lines. In the tropical Atlantic, for example, Frank (1978) found that the most significant differences between squall lines and nonsquall cloud clusters were that the former tended to propagate faster and were accompanied by about twice the low to midtropospheric shear. In a study of severe squall line formation in Oklahoma,

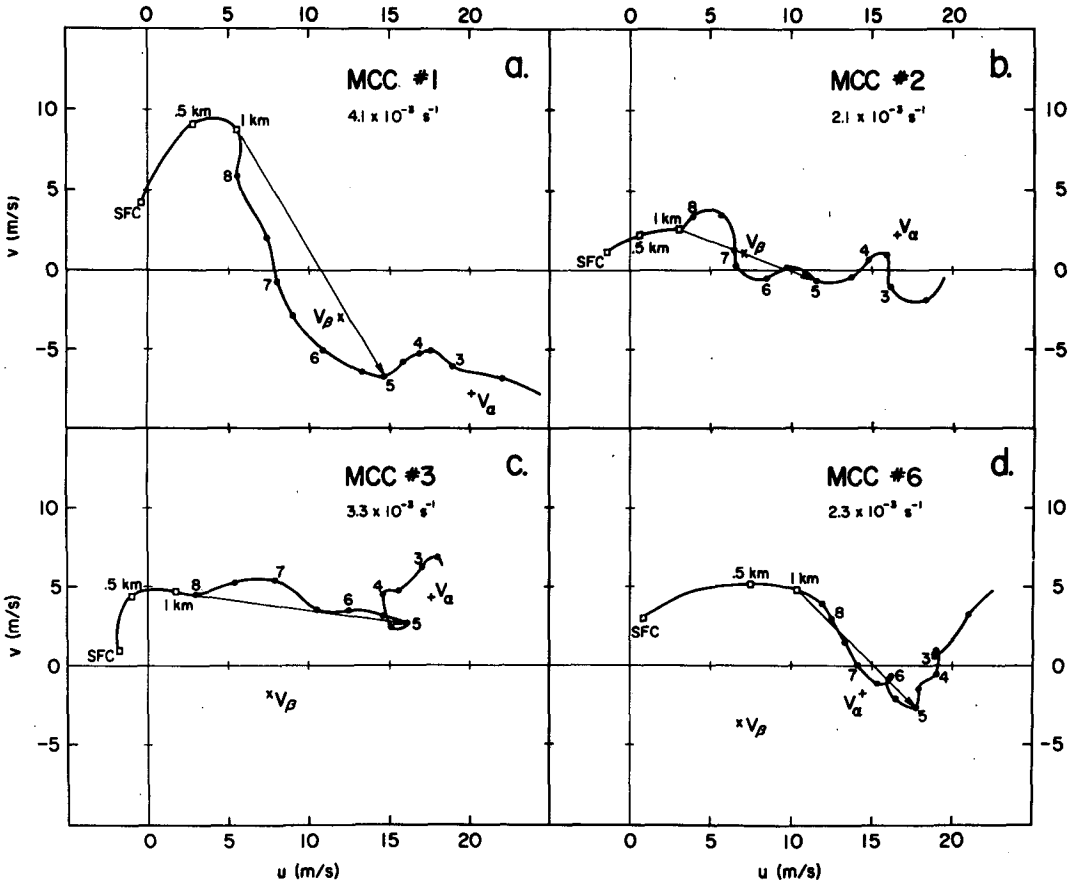

FIG. 13. Environmental wind hodographs for MCCs numbers 1, 2, 3 and 6 (a–d, respectively). Winds are depicted at the surface and at 0.5 and 1.0 km above the surface, and are averaged over 50-mb layers above that (labeled in hundreds of mb). For each MCC, rawinsonde tracking winds from the four nearest NWS stations at 0000 GMT were averaged, winds from the nearest seven to nine stations at 1200 GMT were averaged, and the resultant two sets of wind were averaged to produce the hodograph. For the later-occurring MCC number 6 (Fig. 4), the 1200 GMT set was weighted twice. The magnitude of the depicted 1.0 km–500 mb shear vector is indicated. Also shown are the velocity of the −53°C IR area centroid (V_α) and the mean velocity of the meso-β convective features (V_β), both computed over the MCC "start-to-maximum" period. In deriving V_β, mean 2-h velocities were first computed from the displacements of the meso-β features (including stationary features) in Figs. 6, 8, 10 and 12, and these 2-h velocities were then averaged over the appropriate period.

Bluestein and Jain (1985) found that average shear in the surface to 6-km layer ranged upward from 3.3 $\times 10^{-3}$ s^{-1} for four classes of squall lines. Johns and Hirt (1983) observed that stronger shear aids the development and fast movement of derecho-type squall lines. Finally, Weisman and Klemp (1984) performed a series of numerical simulations that show the effect of varying shear profiles on the evolution of cumulonimbus. They demonstrated that convection in low shear is relatively short-lived, while increasing, directionally varying shear favors successive storm splitting towards a coherent, faster-moving squall line organization (their strongest-shear case resulted in supercell formation, which is consistent with the stronger shears reported by Bluestein and Jain, 1985, for isolated supercells).

Active cold fronts also affected the substructure of several MCCs in the episode. This controlling influence was manifested by the development of meso-β convective bands oriented parallel to the front, and their eastward translation as a relatively steady-state entity along the moving front. This characteristic was seen in the decaying stages of MCC 2 (cluster G in Fig. 8f) and through most of MCC 3 (clusters D–F, and then L, in Fig. 10c–f).

A major difference between the large western and eastern MCCs was that the latter tended to continuously regenerate intense convective elements on the southwestern flank (as with clusters A and G in Fig. 12), whereas convective-scale propagation in the western cases was generally on an eastern (or forward) flank. Thus, in the eastern MCCs, the eastward component of V_β (Fig. 13d) was due largely to the eastward expansion of meso-β components by the translation of weakening convective elements, while a preferred location for large rainfall accumulations was on the southwestern flank of the meso-α system. This persistent rear-flank location for convective regeneration was also likely responsible for the slower V_α, relative to the upper-tropospheric flow, than in the western cases (Fig. 13).

There are several factors that likely contributed to this difference. First, for the eastern systems, the strong westerly component of the low-level jet resulted in the strongest relative inflow of moist, unstable air being on the southwestern flank of the meso-β convective features (Fig. 13d); for the western systems, the sloping plains constrain the low-level jet to be more southerly, resulting in an easterly component of relative inflow to the meso-β components (Fig. 13a–c). Second, more widespread low-level moisture was available for the eastern systems, versus the consistent west-to-east (high-to-low elevation) moisture gradient for the western systems. Finally, more pronounced forcing on the eastern flank of the western systems, due to a downsloping density current, may have contributed to their more pronounced eastward propagation. In any event, the western MCCs, with their more numerous meso-β convective components and nonstationary propagation modes, displayed more chaotic and random

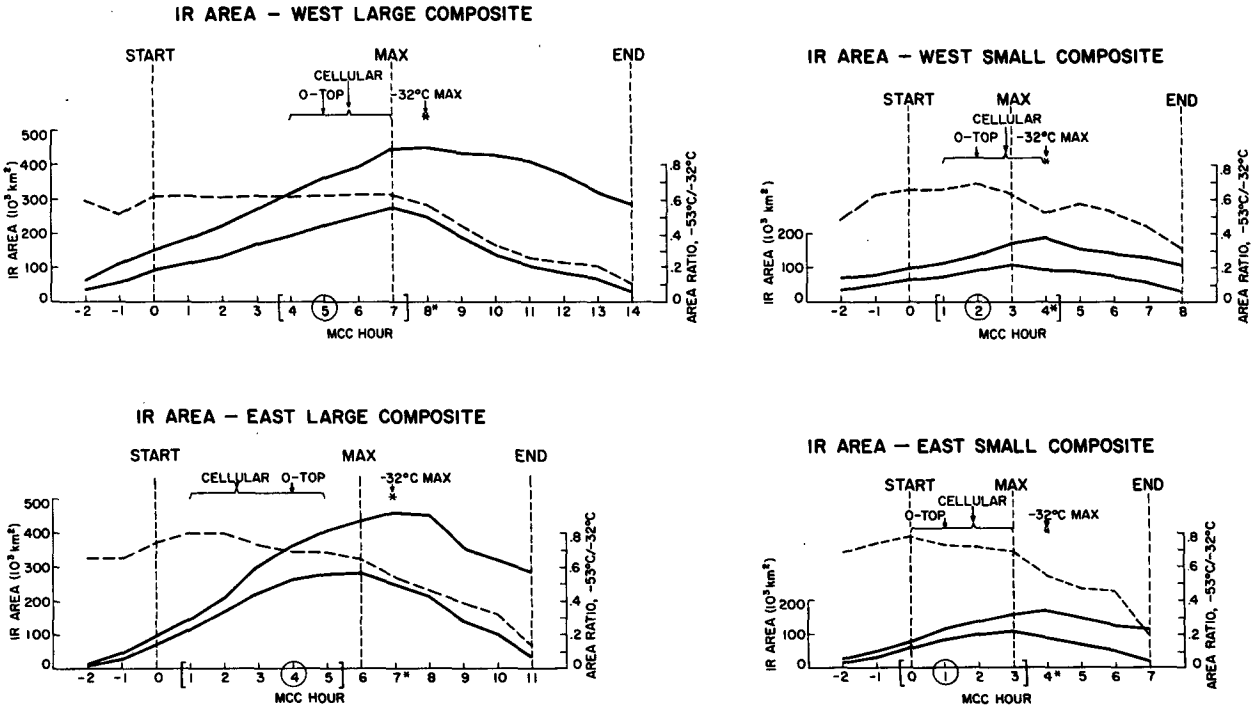

FIG. 14. Trends of composite-MCC anvil size, as defined by areas of cloud-top IR temperature colder than −32° and −53°C (upper and lower solid curves, respectively). Ratio of −53° to −32°C areas is given by the dashed line. IR features of the composites are as in Fig. 4.

patterns of development in their internal substructures, than the eastern systems.

Note in Fig. 13 that for each system, the magnitude of V_α is about twice that of V_β. In the substructure analyses, it was apparent that this was not simply due to the anvil's downwind expansion from the meso-β clusters producing it, because successive meso-β clusters were seen to exist within the core and help sustain the meso-α system. Thus, regardless of their variable substructure, these large MCCs may be characteristic of a meso-α disturbance, with phase speed V_α, which helps trigger the successive development of meso-β clusters, which in turn help sustain the meso-α system through their discrete propagation.

5. Meso-β-scale precipitation characteristics of the MCCs

The previous section demonstrates that despite the characteristic meso-α-scale evolution of the MCC's cloud shield (as typified by the satellite sequence in Fig. 2), there is a complex case-to-case variability in its radar substructure. The hourly precipitation patterns and amounts display a corresponding variability. Rockwood et al. (1984) present these characteristics for a particular dual MCC case. To avoid becoming mired in the details of the individual MCCs in this episode, we have adopted the composite analysis approach described in Section 3c (see Table 1 and Fig. 4). The resultant composite analyses, while losing the spatial complexity inherent in the individual systems, retain important temporal variations that allow generalizations to be made concerning the western/eastern and large/small MCCs. Because of our limited sample size, no statistical significance tests have been made, and our interpretation of these variations is qualitative.

The growth/decay cycle of the IR cloud shield associated with each composite MCC is displayed in Fig. 14. For all composites, both −53° and −32°C areas expand monotonically to their maximum sizes, followed by monotonic decreases. The major difference between the two large composites is that the E-L system has a much larger expansion rate in its first several hours, and attains a meso-α "cellular" organization much sooner, than the slower developing W-L MCC.

Comparing the large and small systems, both large composites have early growth rates exceeding those of their smaller and shorter-lasting counterparts. For example, over the organizational period from MCC hours −2 to 2, the normalized growth rates of the −53°C area in the W-L and E-L systems are 123% and 169% of the W-S and E-S rates, respectively. This suggests a potential short-range forecasting technique whereby the maximum size and duration of an MCC might be projected from its early growth trend.

For each composite, the expansion rates of the −32° and −53°C areas are fairly constant from "start-to-maximum", with the ratio of −53° to −32°C areas remaining relatively steady at about 0.6 to 0.8. After the "maximum", the −32°C area continues to expand for another hour, and the ratio decreases steadily to the "end". This single growth/decay cycle was characteristic of the individual MCCs, and supports the view that the mature MCC develops an organized meso-α-scale vertical circulation (Maddox, 1980); a system less organized on the meso-α-scale and more dominated by convective-scale circulations might be expected (if it could produce a large contiguous anvil at all) to produce a more pulsating anvil with multiple maxima of cold IR areas during its extended duration.

Just as the maximum −53°C area is reached 1 h prior to the maximum −32°C area in all composites, the "overshooting-top-maximum", with an interior region of cloud-top temperatures considerably colder than −53°C, occurs about 2 h prior to the maximum −53°C area. Thus, to the extent that cloud top temperatures represent the intensity of vertical motions, there is evidence that the MCC transforms steadily from a relatively small system dominated by intense convective circulations into a larger system of diminishing vertical motions.

For each individual MCC, the accumulated rainfall volume over MCC hours −2 to "end" +1 is listed in Table 1 as a measure of total storm rainfall production. While the W-L and E-L MCCs produced anvils about 2.5 times larger than their smaller counterparts, their average rainfall volumes were 13.6 and 4.6 times greater, respectively, than that of the smaller systems' averages. This can only be partly accounted for by the larger systems' longer durations (by factors of 1.8 and 1.5, respectively) and their larger time-averaged anvil areas (by about a factor of 2). Thus, there is evidence that large MCCs are more efficient precipitators than smaller systems. This is particularly evident for the western cases, where one might expect significant subcloud evaporation of precipitation in this more arid region. Indeed, the W-S MCC number 5a produced no recorded rainfall for 2 h of its meso-α "cellular" period. A probable contributor to the larger systems' greater efficiency is that the cross-sectional area–to–circumference ratio of their precipitation-producing cloud area is larger, which implies a correspondingly large ratio of protected "core" precipitation to "peripheral" precipitation, the latter being more susceptible to evaporation in the subsaturated environmental air.

Quartiles of total rainfall volume were computed for each individual MCC. Their timing is shown in Fig. 4. Within the W-L and E-L categories, note that the quartiles are timed fairly consistently with respect to the IR features. Thus the composite precipitation analyses presented below accurately reflect the nature of the individual large systems. In contrast, there is much less consistency in the timing of the quartiles in both small MCC categories. While this is likely due in part to more serious sampling problems (i.e., fewer affected stations), it also likely reflects an inherent greater variability of these "smaller-scale" and less precipitation-

efficient MCCs. Thus, the small MCC composites presented below reflect less accurately the individual systems.

Figure 15 depicts the precipitation trend for each composite MCC in terms of average hourly rain rate, area and volume ($\bar{R}$, $\bar{A}$ and $\bar{V}$). For the W-L and E-L MCCs, the graphs indicate that maximum $\bar{R}$ occurs early in the intense growth phase of the MCC, followed by a steady decrease that tends to level off in the latter decaying stage. The $\bar{A}$ increases steadily until 1–2 h after the MCC "maximum" and near the −32°C maximum, followed by a steady decrease. The resultant $\bar{V}$ maximizes 1–2 h prior to the "maximum", towards the end of the meso-α "cellular" stage and near or shortly after the "overshooting-top maximum". From the quartiles of accumulated precipitation volume shown in Fig. 4, it can be seen that the peak in $\bar{V}$ occurs about 1 h prior to the 50% quartile.[8]

The hourly precipitation volumes in Fig. 15 are partitioned between "core" and "peripheral" rainfall, the former being due to those hourly precipitation envelopes (section 3c) that were half or more within the −53°C IR area at both the beginning and end of the hour. The great majority of the MCC's rainfall occurs within its "core" region. Note that the maximum rain area, about 12×10^4 km^2 for both large composites, is less than half the maximum −53°C area seen in Fig. 14, indicating that most of the MCC anvil is nonprecipitating. Only during the last few hours, as the −53°C area shrinks to sub-MCC dimensions, does the diminishing rainfall become appreciably "peripheral".

The small composite MCCs in Fig. 15 show comparable trends in $\bar{R}$ and $\bar{A}$, which maximize early and relatively late, respectively, in the life-cycles. The magnitudes of $\bar{R}$ are also comparable to those of the large systems. The smaller areas affected, however, result in much smaller volumes, which exhibit a much less pronounced growth/decay trend than seen in the large MCCs. The disproportionally low rainfall areas and volumes, relative to the IR anvil areas, of the small MCCs compared to the large systems (especially for the western composites) again suggest that the larger MCCs are more precipitation-efficient.

A more detailed examination of the average hourly rainfall rates depicted in Fig. 15 was made by deriving frequency distributions of reported rainfall intensities in the manner discussed in section 3c. The resulting distributions for the 2.5-mm and 0.25-mm gages are illustrated in Figs. 16 and 17, respectively. Due to the small sample size (number) in the early hours of the large composites and through much of the small (especially W-S) composites, the distributions and their average intensity ($\bar{R}$) are questionable at these times. Still, reasonably consistent trends emerge from the analyses.

For the large MCCs, the maximum average rates in the early growth stage (Fig. 15) are shown in both gage-type distributions to be due to the relative maximum frequency of the heavier hourly rates, including reports exceeding 51 mm. In Fig. 16, for example, the percentages of hourly reports $\geqslant$ 12.7 mm reach maxima of 25% at MCC hour 5 and 43% at hour 1 for the W-L and E-L composites, respectively. After these maxima, the decreasing fraction of intense rainfall represents the weakening of the meso-β clusters that built the meso-α complex. The meso-α system nevertheless continues to expand for several more hours, becoming increasingly dominated by the lighter rainfall intensities.

While the W-S MCC shows a similar tendency in both Figs. 16 and 17, the E-S composite presents a less consistent trend, with intense rates persisting through most of its maturity in Fig. 16. This discrepancy between the two E-S distributions is likely a combination of inadequate sampling and variability between the individual systems. In Fig. 4, for instance, the quartiles of accumulated precipitation volume for the E-S MCCs numbers 4 and 9 indicate that much more of their rainfall occurred later in their life-cycles than was generally the case for the other MCCs.

A similar frequency distribution analysis, utilizing the Manually Digitized Radar (MDR) data, is shown in Fig. 18 and corroborates the findings of the rainfall distributions. For each composite, the relative frequencies of intense "convective" MDR values (code thresholds 6 and 8 in Table 2) are high through the initial developing stage of MCC growth, remaining high until or maximizing in the early meso-α "cellular" stage. The relative frequency of these high values decreases thereafter, with an increasing proportion of MDR values less than 6. The secondary peaks during the latter half of the E-S composite reflect the relatively late-occurring heavy rainfall of MCCs number 4 and 9.

Note that the areas of nonzero MDR coverage in Fig. 18, scaled to the number of nonzero blocks, are considerably larger than the hourly rainfall areas in Fig. 15, and are in fact much more comparable to the IR anvil areas in Fig. 14. This does not imply that echo coverage is complete over the anvil area, because an MDR box received a nonzero value if any fraction of it contained echo. However, it does indicate that echo, whether solid or patchy, is distributed over an area that approaches the anvil size. The much smaller rainfall areas in Fig. 15 are likely due to the patchiness of this echo, some of the precipitation being too light to be

[8] This analysis of hourly $\bar{A}$, $\bar{R}$ and $\bar{V}$ values treated data from both types of gages as a single sample in order to maximize the sampling. However, with its higher recording threshold, a 2.5-mm gage records precipitation (particularly light rainfall) less accurately than a 0.25-mm gage. For the large MCCs, similar composite analyses were done using each gage type separately. This comparison indicated that the effect of the less accurate gage on the combined-gage analysis was towards systematically lower $\bar{A}$ values and higher $\bar{R}$ values, and vice-versa for the 0.25-mm gages. However, the trends in $\bar{A}$ and $\bar{R}$ for both samples were similar to those depicted in Fig. 15. Also, the resultant hourly $\bar{V}$ values (and trends in $\bar{V}$) in the comparative analyses were not significantly different from the combined-gage analysis: a smaller/larger $\bar{A}$ times a larger/smaller $\bar{R}$ yielded similar values of $\bar{V}$.

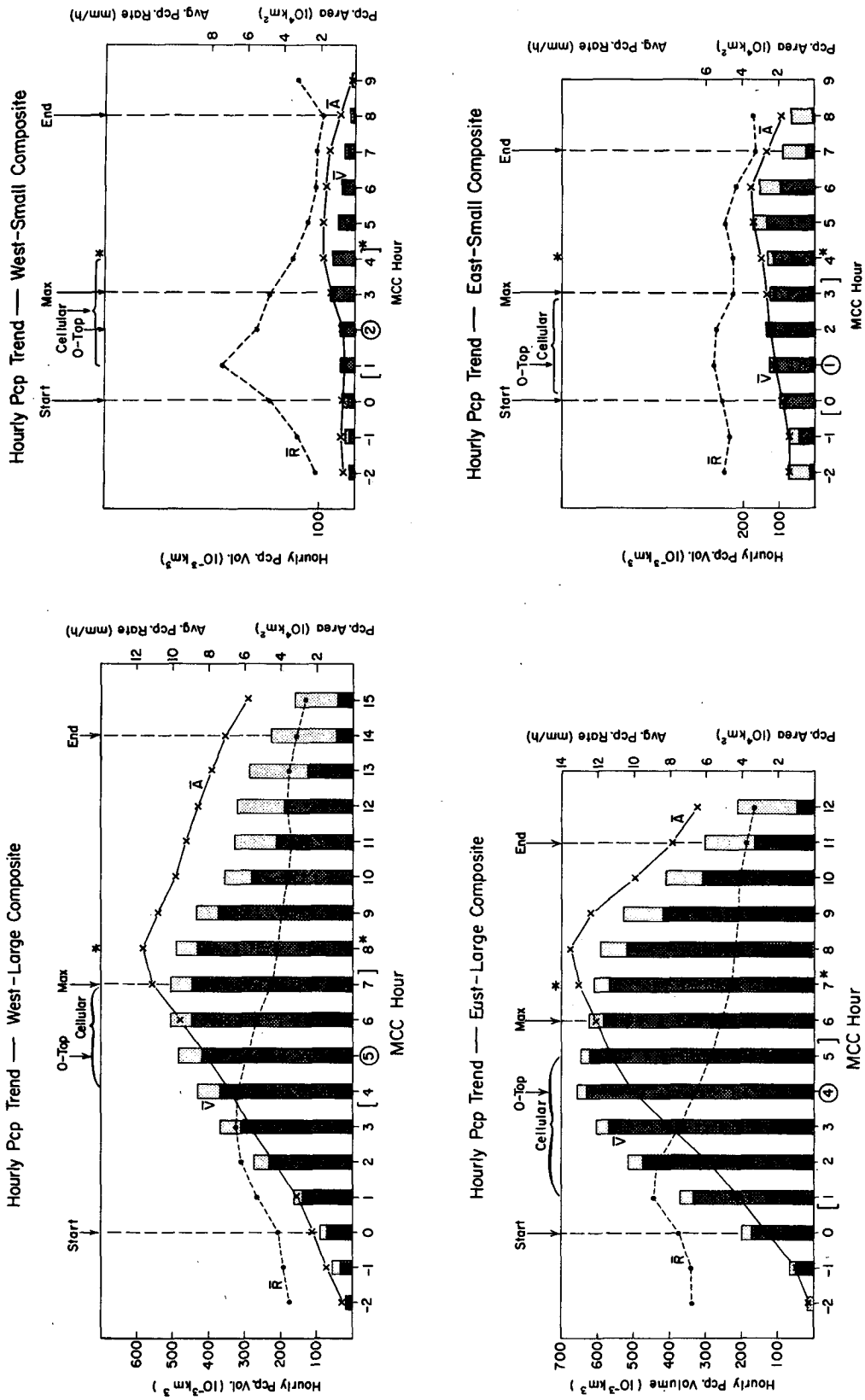

FIG. 15. Trends of composite-MCC measurable hourly precipitation area ($\bar{A}$, solid line), average hourly precipitation rate ($\bar{R}$, dashed line) and hourly precipitation volume ($\bar{V}$, bars). Precipitation volumes are partitioned between "core" and "peripheral" rainfall (dark and light shaded portions, respectively, and defined in text). Hourly values are plotted at the end of the hour to which they apply. Noted IR features are as in Fig. 4.

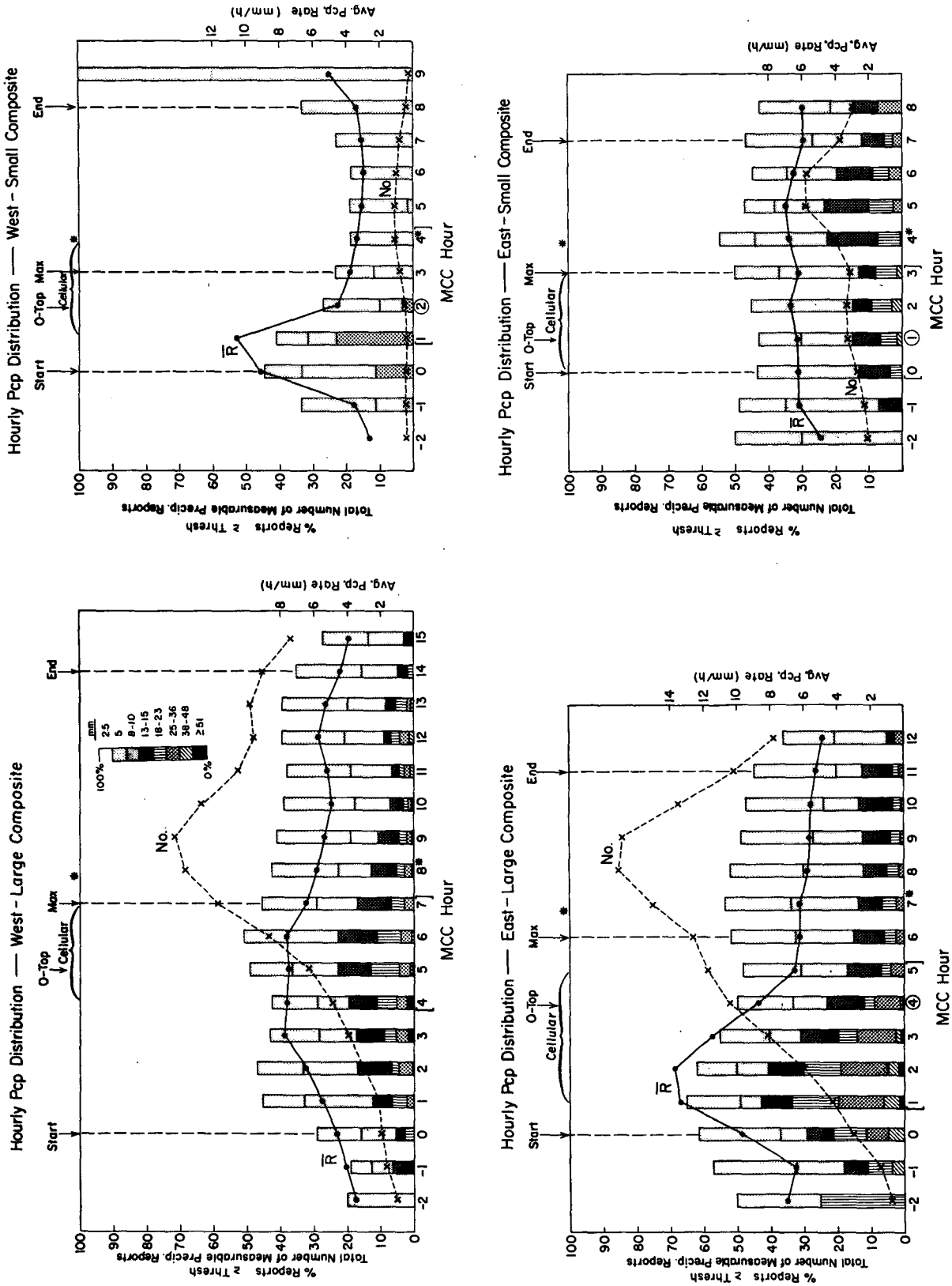

FIG. 16. Trends of composite-MCC frequency distributions of measurable hourly precipitation reports over various intensity categories, utilizing raingages with increments of 2.5 mm. Bars are partitioned into percentages of measurable reports contributed by each intensity category, shaded according to the key inset in the west-large composite. The contribution due to the lightest intensity category (reports of 2.5 mm) is represented by the distance from 100% line down to the top of the partitioned bars. The total sample size for each hour (number) is the number of measurable reports summed over the three MCCs, and is plotted as the solid line. Other details are as in Fig. 15.

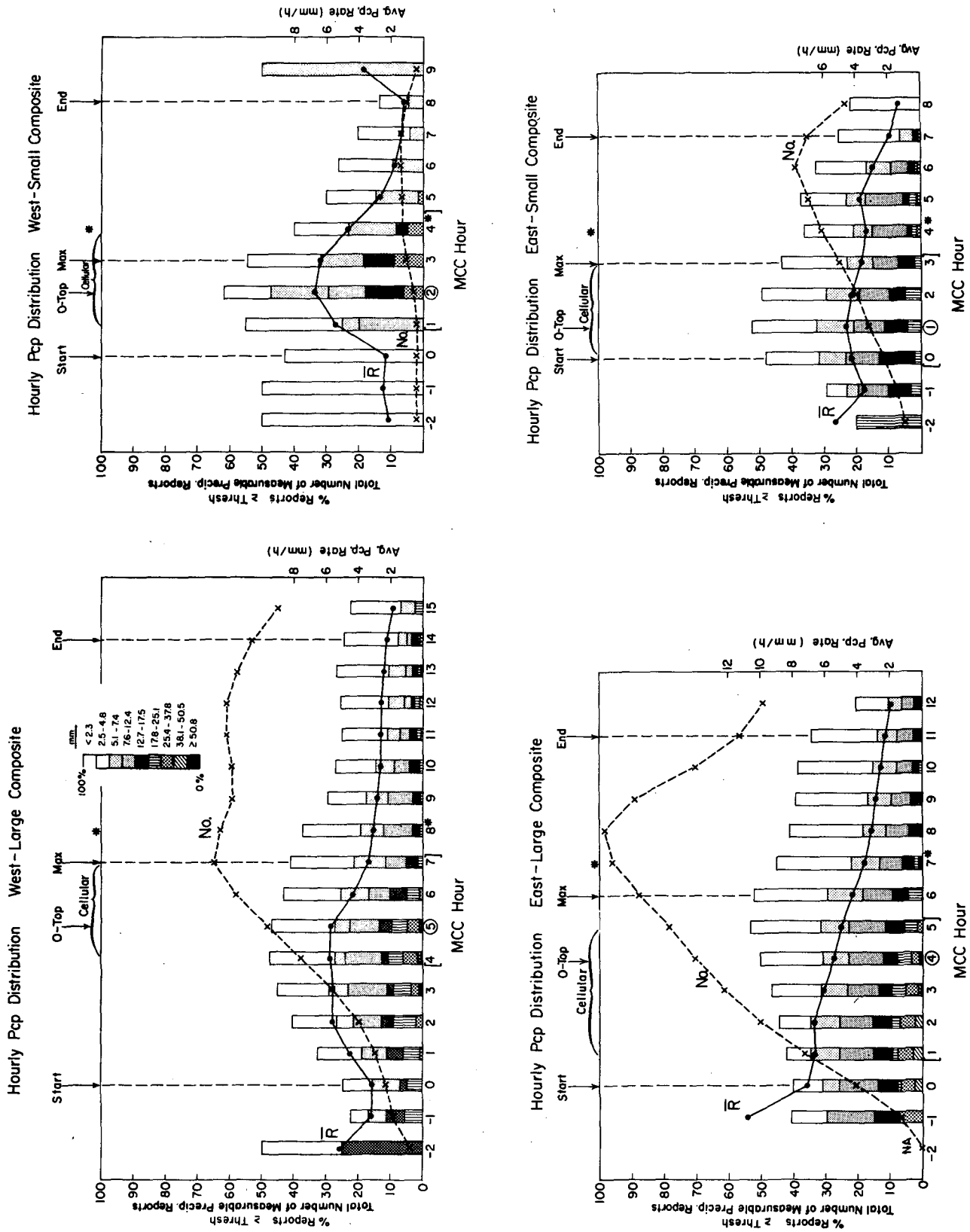

FIG. 17. Trends of composite MCC-frequency distributions of measurable hourly precipitation reports over various intensity categories, utilizing raingages with increments of 0.25 mm. Details are as in Fig. 16, except the lightest intensity category is for reports from 0.25 to 2.29 mm.

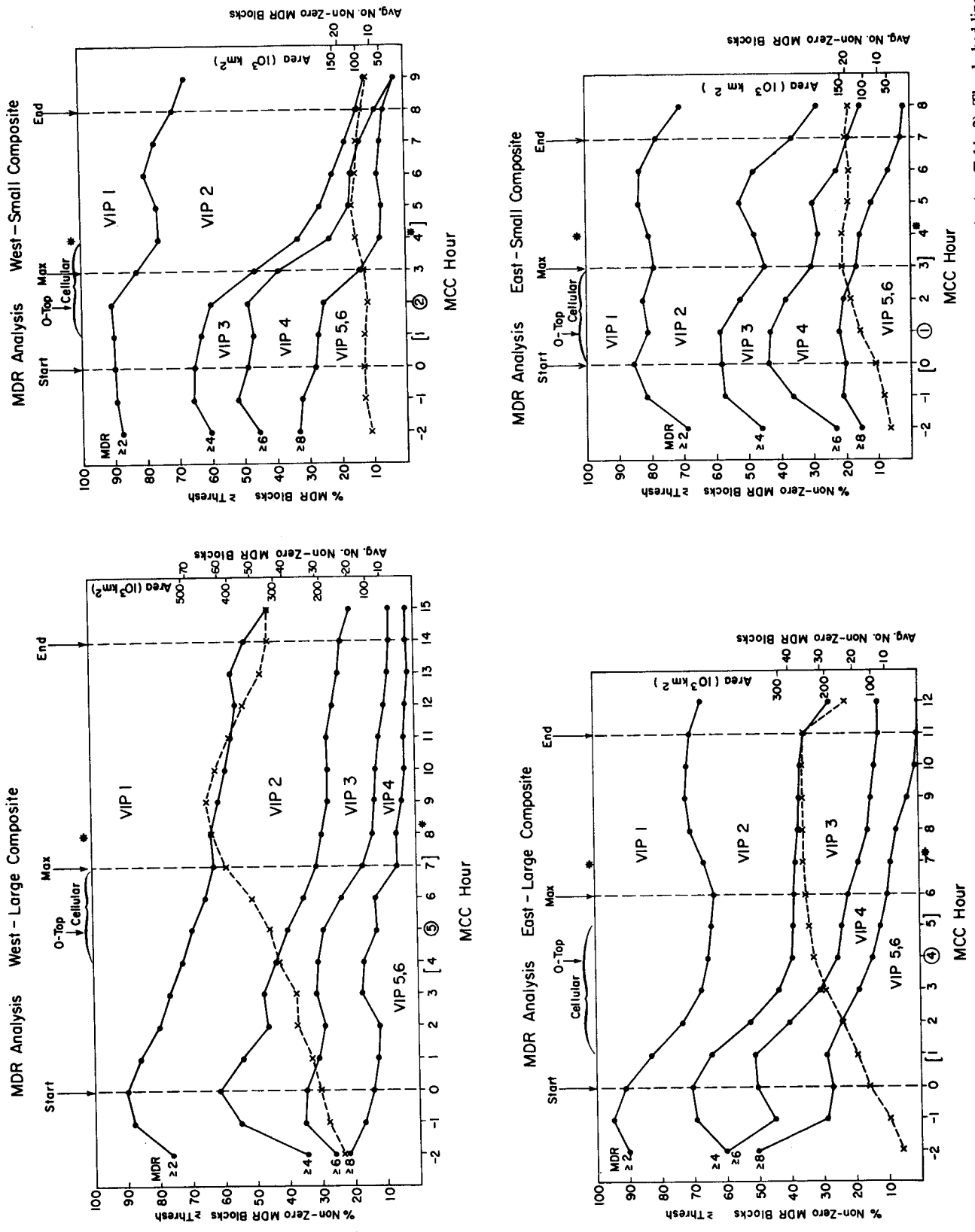

FIG. 18. Trends of composite-MCC frequency distributions of nonzero Manually Digitized Radar (MDR) blocks over various intensity categories (see Table 2). The dashed line gives the average number of nonzero MDR blocks, which is scaled to areal coverage on the right ordinate. Hourly values, applicable at about 30 min off the hour, are plotted at the end of that hour. The east-large composite includes data for MCC numbers 6 and 9/10 only, as no data were available for MCC number 8.

recorded, and the evaporation of some of the precipitation below the 0.5–1.0° scanning angles. At these angles the radars are sampling up to several kilometers in altitude at far ranges, which suggests that some of the echo coverage is due to precipitation particles aloft in the anvil which never reach the surface.

From the analyses presented in Figs. 4 and 14–18, a fairly clear picture of MCC precipitation evolution emerges, particularly for the "better-behaved" large MCCs. The maximum relative occurrence of intense rainfall rates near the beginning of the meso-α "cellular" period and near the "overshooting-top maximum", and their subsequent decrease through the remainder of the "cellular" stage, imply that the intense convection producing these intense rates is necessary for the development of the organized meso-α circulation, which then persists as a several-hour response to that forcing. During that response, the MCC is transformed into a larger precipitating system of increasingly lighter and more stratiform anvil rainfall, and then gradually decreases in size as it decays. This life-cycle is consistent with that discussed by Kane et al. (1985) in their composite analysis of MCC precipitation.

The relationship between the enhanced IR cloud-top features and the concurrent rainfall characteristics of these MCCs is qualitatively consistent with empirical convective rainfall nowcasting techniques that rely on anvil expansion rates, cloud-top temperatures and cloud histories (Scofield and Oliver, 1977; Griffith et al., 1978). Moreover, inasmuch as these composites represent typical MCC life cycles, the relation of the IR and precipitation trends in Figs. 14–18 provides a potential tool for forecasting certain aspects of the latter ⅔ of the MCC's life cycle, especially for "better-behaved" large systems.

For example, the real-time observation via satellite and radar (or raingages) of the formation of a growing, incipient MCC (MCC hour 0) would portend the increase or continuation of intense convective rainfall over the next 2–4 h, and a longer steady increase in both precipitation area and volumetric rainfall rate. Continuing into the life cycle, the observation of a decrease in relative frequency of intense convection within an organized, "cellular" MCC would signal a 2–3 h longer expansion of the system and persistence of its "cellular" stage, followed by its gradual decay. From the standpoint of average precipitation intensity in Fig. 15, such decreasing trends might be reliably established in real time over the period of MCC hours 3 to 5 for the W-L MCC, and hours 1 to 3 for the E-L system. As a hydrological forecasting tool, that determination would permit the projections of maximum volumetric rain rate of the system to occur over the next 1–2 h and active precipitation area to increase over the next 3–5 h. A further precursory indicator of those projected maxima would be the first signs of the IR cloud shield showing weakening in its "overshooting top" intensity (evident by MCC hours 6 and 5, respectively, for the W-L and E-L composites). After a decreasing trend is observed over a 1–2 h period following the maxima in any of the volume, area or average intensity trends, the curves suggest that simple extrapolation techniques could project these trends for several hours through the MCC's dissipation.

6. Summary and discussion

Based on an analysis of an 8-day episode of MCCs over the central United States, a number of generalizations are inferred concerning their structural evolution. These include

1) Thunderstorms in the MCCs were generally well-organized into meso-β-scale convective clusters or bands. The large MCCs had multiple meso-β components throughout their life cycle, whereas the smaller MCCs tended to be dominated by a single meso-β component.

2) The large western MCCs developed on the High Plains as a result of the growth, interaction and merger of several meso-β convective features. A confluent environmental flow at 700 mb appeared to aid this development. The meso-β components tended to originate along larger, meso-α-scale axes, such as the eastern slopes of the Rockies, surface troughs and fronts, and extensive mesoscale outflow boundaries.

3) In the large western cases, more than one meso-α axis as described above was important. The region of most intense meso-β convective development and rapid MCC growth occurred near the point where these meso-α axes intersected. This appears to be a larger-scale analog to what Purdom (1979) has inferred from satellite imagery: convective development is preferred along discontinuities, such as fronts, arc cloud meso-high boundaries, and dry lines, and is especially favored at the intersection of two of these features.

4) The large eastern MCCs, generated in Iowa and Missouri, involved fewer discrete meso-β components in their formation, tending instead to grow up-scale from one or two vigorous meso-β convective clusters. However, they also developed at the intersection of two meso-α axes.

5) In both eastern and western regions, meso-α discontinuities produced by previous MCCs affected the evolution and structure of new systems.

6) The configuration and development of meso-β clusters were more chaotic and random in the large western MCCs, unless there were strong environmental controls, such as an active cold front or strong vertical wind shear. The former favored relatively steady-state meso-β bands oriented parallel to the front, and the latter favored a rapidly moving squall line structure. The less chaotic nature of the large eastern MCC substructure may be related to the fewer intense meso-β clusters that were involved in their genesis and a more saturated subcloud environment, which together would produce fewer and less vigorous storm outflows that

could interact in the manner described by Purdom (1979).

7) In the absence of strong controlling influences (such as fronts), the decay of the large MCCs was characterized by (or perhaps caused by) the divergent tracking between its meso-β elements.

8) The phase speed of the large MCCs was about twice the mean phase speed of their multiple meso-β components. The meso-α disturbance thus appeared to be sustained by the discrete propagation of meso-β elements, which perhaps in turn were triggered by the meso-α disturbance.

9) The precipitation produced by the MCCs was largely confined to the meso-β convective features, particularly for the western systems. Though the cold, uniform cloud shield may be indicative of mid- to upper-tropospheric meso-α-scale ascent and precipitation generation, the area and amount of precipitation reaching the surface was appreciably reduced, due likely in part to significant subcloud evaporation.

These generalizations are drawn from only a few MCCs occurring in a quasi-steady synoptic pattern, and thus may not be representative of MCCs in different synoptic conditions, in different geographical regions, or earlier or later in the convective season. For instance, Clark et al. (1980) and Merritt and Fritsch (1984) discussed several classes of organized mesoscale convection that can meet the MCC criteria, but each type was associated with a distinct synoptic pattern which exerted strong controls on the internal organization of the storm. Indeed, the cases discussed here and those recently described by others (Leary and Rappaport, 1983; Rockwood et al., 1984; Smull and Houze, 1985) indicate that there is extreme variability in the internal structure and evolution of MCCs.

Nevertheless, the net result in each case is a long-lived meso-α-scale system that develops from more localized, intense convective forcing. By averaging through the internal complexity of the MCCs, an analysis of hourly precipitation statistics has shown that this evolution is characterized by a well-defined precipitation life cycle relative to the satellite appearance, especially for the larger MCCs. Average precipitation rates, and the fraction of precipitation due to intense rainfall rates, increase through the initial developmental stage and reach their peak near the time that the MCC attains an organized, meso-α-scale "cellular" appearance. The essential up-scale transformation into an intense MCC has thus occurred by this time, which is still early in the life cycle. During the several-hour intense meso-α "cellular" stage, the volumetric rain rate of the MCC reaches a well-defined maximum, which may reflect the maximum intensity of its meso-α-scale circulation. Shortly after this maximum, the MCC reaches its maximum size (−53°C IR area) and loses its meso-α "cellular" appearance. Though the active rain area continues to expand a while longer, it is characterized by increasingly lighter rain and is apparently indicative of a prolonged, weakening mesoscale circulation.

This life cycle resembles closely that discussed by Leary (1984) and generalized by Houze and Betts (1981) for mesoscale precipitation features in the tropical Atlantic. In the latter review, it was hypothesized that the strong convective forcing maximizes about a third of the way through the feature's typical 12-h lifecycle, the latter two-thirds being a prolonged mesoscale response. It seems likely that useful hydrological forecasting techniques could be developed on the basis of this extended response to real-time observable events. In those MCCs having multiple meso-β-scale convective features, it remains unclear to what extent each feature undergoes a similar life cycle independently, or whether they interact dynamically in a way that appreciably affects the entire meso-α-scale system.

Acknowledgments. Dr. Peter J. Wetzel performed some of the preliminary analysis incorporated into this study. Reviews by John F. Weaver, Michael A. Fortune and anonymous readers helped us to finalize the paper. The satellite data covering the MCC episode were provided by Dr. Aylmer H. Thompson. We thank Lucy McCall and Judy Sorbie for their drafting services and Brenda Thompson for processing the manuscript. This research was supported under National Science Foundation Grants ATM-7908297 and ATM-8312077, by the National Aeronautics and Space Administration under Contract NSG-5341, and by the Office of Naval Research under Contract N00014-83-K-0321. It was also supported in part by the Air Force Office of Scientific Research under AFOSR Grant 82-0162 and by the National Oceanic and Atmospheric Administration under Grant NA81RAH00001.

REFERENCES

Bergeron, T., 1968: Cloud physics research and the future fresh-water supply of the world. *Proc. Int. Conf. on Cloud Physics,* Toronto, Int. Union Geod. Geophys., p. 9.12.

Bluestein, H. B., and M. H. Jain, 1985: Formation of mesoscale lines of precipitation: Severe squall lines in Oklahoma during the spring. *J. Atmos. Sci.,* **42,** 1711–1732.

Bosart, L. F., and F. Sanders, 1981: The Johnstown Flood of July 1977: A long-lived convective system. *J. Atmos. Sci.,* **38,** 1616–1642.

Clark, J. D., Ed., 1983: *The GOES User's Guide.* U.S. Dept. Commerce, National Oceanic and Atmospheric Administration, National Environmental Satellite, Data, and Information Service, Office of Satellite Data Processing and Distribution, 167 pp. [NTIS No. PB84-104413].

——, A. J. Lindner, R. Borneman and R. E. Bell, 1980: Satellite observed cloud patterns associated with excessive precipitation outbreaks. *Preprints, Eighth Conf. on Weather Forecasting and Analysis,* Denver, Amer. Meteor. Soc., 463–473.

Cotton, W. R., R. L. George, P. J. Wetzel and R. L. McAnelly, 1983: A long-lived mesoscale convective complex. Part I: The mountain-generated component. *Mon. Wea. Rev.,* **111,** 1893–1918.

Forbes, G. S., and R. M. Wakimoto, 1978: Downbursts and tornadoes of 6 August 1977 near Springfield, Illinois. Satellite and Meso-

meterology Research Paper No. 161, Dept. of Geophysical Sciences, University of Chicago, 50 pp. [NTIS No. PB80-159791].

——, and ——, 1983: A concentrated outbreak of tornadoes, downbursts and microbursts, and implications regarding vortex classification. *Mon. Wea. Rev.*, **111**, 220–235.

Frank, W. M., 1978: The life-cycles of GATE convective systems. *J. Atmos. Sci.*, **35**, 1256–1264.

Fritsch, J. M., and R. A. Maddox, 1981: Convectively driven mesoscale weather systems aloft. Part I: Observations. Part II: Numerical simulations. *J. Appl. Meteor.*, **20**, 9–26.

Fujita, T. T., 1981: Tornadoes and downbursts in the context of generalized planetary scales. *J. Atmos. Sci.*, **38**, 1511–1534.

Gray, W. M., and R. W. Jacobson, Jr., 1977: Diurnal variation of deep cumulus convection. *Mon. Wea. Rev.*, **105**, 1171–1188.

Griffith, C. G., W. L. Woodley, P. G. Grube, D. W. Martin, J. Stout and D. N. Sikdar, 1978: Rain estimation from geosynchronous satellite imagery—Visible and infrared studies. *Mon. Wea. Rev.*, **106**, 1153–1171.

Houze, R. A., Jr., and A. K. Betts, 1981: Convection in GATE. *Rev. Geophys. Space Phys.*, **19**, 541–576.

Johns, R. H., and W. D. Hirt, 1983: The derecho . . . A severe weather producing convective system. *Preprints, 13th Conf. Severe Local Storms*, Tulsa, Amer. Meteor. Soc., 178–181.

Kane, R. J., Jr., C. R. Chelius and J. M. Fritsch, 1985: The precipitation characteristics of mesoscale convective weather systems. *Preprints, Sixth Conf. on Hydrometeorology*, Indianapolis, Amer. Meteor. Soc., 205–211.

Kessler, E., Ed., 1982: *Thunderstorms: A Social, Scientific, and Technological Documentary. Vol. 2: Thunderstorm Morphology and Dynamics.* U.S. Dept. of Commerce, National Oceanic and Atmospheric Administration, Environmental Research Laboratories, 603 pp. [U.S. Govt. Printing Office, Washington, DC 20402, Accession No. C55/602/T42/v.2].

Kincer, J. B., 1916: Daytime and nighttime precipitation and their economic significance. *Mon. Wea. Rev.*, **44**, 628–633.

Leary, C. A, 1984: Precipitation structure of the cloud clusters in a tropical easterly wave. *Mon. Wea. Rev.*, **112**, 313–325.

——, and R. A. Houze, Jr., 1979: The structure and evolution of convection in a tropical cloud cluster. *J. Atmos. Sci.*, **36**, 437–457.

——, and E. N. Rappaport, 1983: Internal structure of a mesoscale convective complex. *Preprints, 21st Conf. on Radar Meteorology*, Edmonton, Amer. Meteor. Soc., 70–77.

Lilly, D. K., 1979: The dynamical structure and evolution of thunderstorms and squall lines. *Ann. Rev. Earth Planet. Sci.*, **7**, 117–161.

McBride, J. L., 1981: Observational analysis of tropical cyclone formation. Part I: Basic description of data sets. *J. Atmos. Sci.*, **38**, 1117–1131.

——, and R. Zehr, 1981: Observational analysis of tropical cyclone formation. Part II: Comparison of non-developing versus developing systems. *J. Atmos. Sci.*, **38**, 1132–1151.

Maddox, R. A., 1980: Mesoscale convective complexes. *Bull. Amer. Meteor. Soc.*, **61**, 1374–1387.

——, 1983: Large-scale meteorological conditions associated with midlatitude, mesoscale convective complexes. *Mon. Wea. Rev.*, **111**, 1475–1493.

——, and C. A. Doswell, III, 1982: An examination of jet stream configurations, 500 mb vorticity advection and low-level thermal advection patterns during extended periods of intense convection. *Mon. Wea. Rev.*, **110**, 184–197.

Merritt, J. H., and J. M. Fritsch, 1984: On the movement of the heavy precipitation areas of mid-latitude mesoscale convective complexes. *Preprints, 10th Conf. on Wea. Forecasting and Analysis*, Clearwater Beach, Amer. Meteor. Soc., 529–536.

Miller, R. C., 1972: Notes on analysis and severe-storm forecasting procedures of the Air Force Global Weather Central. *Tech. Rep. 200 (Rev)*, Air Weather Service (MAC), USAF, 190 pp. [NTIS No. AD-744 042].

Moore, P. L., A. D. Cummings and D. L. Smith, 1974: The National Weather Service Manually Digitized Radar program and its application to precipitation probability forecasting. *Preprints, Fifth Conf. on Weather Forecasting and Analysis*, St. Louis, Amer. Meteor. Soc., 69–74.

Newton, C. W., 1966: Circulations in large sheared cumulonimbus. *Tellus*, **18**, 699–713.

Ogura, Y., and Y.-L. Chen, 1977: A life history of an intense mesoscale convective storm in Oklahoma. *J. Atmos. Sci.*, **34**, 1458–1476.

——, and M.-T. Liou, 1980: The structure of a midlatitude squall line: A case study. *J. Atmos. Sci.*, **37**, 553–567.

Orlanski, I., 1975: A rational subdivision of scales for atmospheric processes. *Bull. Amer. Meteor. Soc.*, **56**, 527–530.

Paegle, J., 1978: A linearized analysis of diurnal boundary layer convergence over the topography of the United States. *Mon. Wea. Rev.*, **106**, 492–502.

Palmen, E., and C. W. Newton, 1969: *Atmospheric Circulation Systems; Their Structure and Physical Interpretation. Int. Geophys. Ser.*, Vol. 13, Academic Press, 603 pp.

Porter, J. M., L. L. Means, J. E. Hovde and W. B. Chappell, 1955: A synoptic study on the formation of squall lines in the north central United States. *Bull. Amer. Meteor. Soc.*, **36**, 390–396.

Purdom, J. F. W., 1979: The development and evolution of deep convection. *Preprints, 11th Conf. on Severe Local Storms*, Kansas City, Amer. Meteor. Soc., 143–150.

Rockwood, A. A., D. L. Bartels and R. A. Maddox, 1984: Precipitation characteristics of a dual mesoscale convective complex. NOAA Tech. Memo. ERL ESG-6, Dept. of Commerce, National Oceanic and Atmospheric Administration, Environmental Research Laboratories, Environmental Sciences Group, Boulder, CO 80303, 50 pp.

Rodgers, D. M., M. J. Magnano and J. H. Arns, 1985: Mesoscale convective complexes over the United States during 1983. *Mon. Wea. Rev.*, **113**, 888–901.

Sanders, F., and K. A. Emanuel, 1977: The momentum budget and temporal evolution of a mesoscale convective system. *J. Atmos. Sci.*, **34**, 322–330.

Schroeder, M. J., and G. E. Klazura, 1978: Computer processing of digital radar data gathered during HIPLEX. *J. Appl. Meteor.*, **17**, 498–507.

Scofield, R. A., and V. J. Oliver, 1977: A scheme for estimating convective rainfall from satellite imagery. NOAA Tech. Memo. NESS 86, U.S. Dept. of Commerce, National Oceanic and Atmospheric Administration, National Environmental Satellite, Data, and Information Service, 47 pp. [NTIS No. PB-270 762/8GI].

Smull, B. F., and R. A. Houze, Jr., 1985: A midlatitude squall line with a trailing region of stratiform rain: Radar and satellite observations. *Mon. Wea. Rev.*, **113**, 117–133.

Toth, J. J., and R. H. Johnson, 1985: Summer surface flow characteristics over northeastern Colorado. *Mon. Wea. Rev.*, **113**, 1458–1469.

Wallace, J. M., 1975: Diurnal variations in precipitation and thunderstorm frequency over the conterminous United States. *Mon. Wea. Rev.*, **103**, 406–419.

Weisman, M. L., and J. B. Klemp, 1984: The structure and classification of numerically simulated convective storms in directionally varying wind shears. *Mon. Wea. Rev.*, **112**, 2479–2498.

Wetzel, P. J., W. R. Cotton and R. L. McAnelly, 1983: A long-lived mesoscale convective complex. Part II: Evolution and structure of the mature complex. *Mon. Wea. Rev.*, **111**, 1919–1937.

Zipser, E. J., 1977: Mesoscale and convective-scale downdrafts as distinct components of squall-line structure. *Mon. Wea. Rev.*, **105**, 1568–1589.